© 2014. Published by The Company of Biologists Ltd | Journal of Cell Science (2014) 127, 3768–3781 doi:10.1242/jcs.149518

RESEARCH ARTICLE

An EMMPRIN–γ-catenin–Nm23 complex drives ATP production and actomyosin contractility at endothelial junctions

Vanessa Moreno[1], Pilar Gonzalo[1], Jesús Gómez-Escudero[1], Ángela Pollán[1], Rebeca Acín-Pérez[1], Mark Breckenridge[2], María Yáñez-Mó[3], Olga Barreiro[1], Fabrizio Orsenigo[4], Kenji Kadomatsu[5], Christopher S. Chen[2], José A. Enríquez[1], Elisabetta Dejana[4], Francisco Sánchez-Madrid[3] and Alicia G. Arroyo[1,*]

ABSTRACT

Cell–cell adhesions are important sites through which cells experience and resist forces. In endothelial cells, these forces regulate junction dynamics and determine endothelial barrier strength. We identify the Ig superfamily member EMMPRIN (also known as basigin) as a coordinator of forces at endothelial junctions. EMMPRIN localization at junctions correlates with endothelial junction strength in different mouse vascular beds. Accordingly, EMMPRIN-deficient mice show altered junctions and increased junction permeability. Lack of EMMPRIN alters the localization and function of VE-cadherin (also known as cadherin-5) by decreasing both actomyosin contractility and tugging forces at endothelial cell junctions. EMMPRIN ensures proper actomyosin-driven maturation of competent endothelial junctions by forming a molecular complex with γ-catenin (also known as junction plakoglobin) and Nm23 (also known as NME1), a nucleoside diphosphate kinase, thereby locally providing ATP to fuel the actomyosin machinery. These results provide a novel mechanism for the regulation of actomyosin contractility at endothelial junctions and might have broader implications in biological contexts such as angiogenesis, collective migration and tissue morphogenesis by coupling compartmentalized energy production to junction assembly.

KEY WORDS: EMMPRIN, Endothelial junctions, γ-catenin, Nm23, Nucleoside diphosphate kinase, NDPK, ATP, Actomyosin contractility, Vascular integrity

INTRODUCTION

A fundamental issue in vascular biology is the understanding of the mechanisms that govern vessel stabilization, because this process is required for development and growth of the organism and because changes in vessel permeability contribute to several pathologies. Vascular integrity depends on the assembly of multicomponent endothelial junctions, the most extensively studied being homophilic VE-cadherin (also known as cadherin-5) interactions at adherens junctions (Dejana, 2004; Giannotta et al., 2013); however, the complete molecular map of the assembly and disassembly of these junctions remains to be defined. Endothelial dynamics largely depend on the spatiotemporal reorganization of the actin cytoskeleton during adherens junction maturation (Smutny et al., 2010) and on the tension that actin filaments, in conjunction with non-muscle myosin II (NM-II), exert over the membrane. This tension actively participates in the expansion from single unstable intercellular cadherin interactions to stable cell contacts involving multiple cadherin pairings (Baum and Georgiou, 2011; Mège et al., 2006; Smutny et al., 2010). Although it is known that non-muscle myosin II (NM-II) contributes to generate the tension required for proper maintenance of linear adherens junctions through several mechanisms (Mège et al., 2006), the spatiotemporal regulation of NM-II-driven tension at cell–cell junctions is just beginning to be elucidated, especially in endothelial monolayers, which experience stronger shear and flow forces than epithelial barriers (Abraham et al., 2009; Ando et al., 2013; Baum and Georgiou, 2011; Conway et al., 2013; Huveneers et al., 2012; Wimmer et al., 2012).

EMMPRIN (extracellular matrix metalloproteinase inducer, also called basigin and CD147) is a glycosylated type-I transmembrane protein of the Ig superfamily (Muramatsu and Miyauchi, 2003), and EMMPRIN molecules are therefore able to engage in homophilic interactions with other monomers and in heterophilic interactions with other partners, such as monocarboxylate transporters, integrins, caveolin-1, CD98, cyclophilins and Shrew1 (Berditchevski et al., 1997; Deora et al., 2005; Schreiner et al., 2007; Tang and Hemler, 2004; Xu and Hemler, 2005). EMMPRIN function has mostly been characterized in relation to tumorigenesis and inflammation (Muramatsu and Miyauchi, 2003). EMMPRIN can also contribute to angiogenesis, the formation of new vessels, in several ways: (1) by endothelial cell activation when present on tumor-derived microvesicles (Millimaggi et al., 2007), (2) by regulation of the PI3K–Akt signaling pathway in activated endothelial cells (Chen et al., 2009) and (3) by modulating the secretion of specific VEGF isoforms (Bougatef et al., 2009). Whether EMMPRIN plays additional roles in the quiescent vasculature has not been investigated.

Here, we report that EMMPRIN orchestrates junction stability *in vitro* and *in vivo* by forming a novel molecular complex at endothelial junctions with γ-catenin (also known as junction plakoglobin) and the nucleoside diphosphate kinase Nm23 (also known as NME1), which provides ATP for the local actomyosin contractility required for proper junction maturation.

RESULTS

Endothelial junctions are altered and vascular permeability enhanced in EMMPRIN-deficient mice

Analysis of mouse tissue sections revealed colocalization of EMMPRIN with the endothelial cell junction marker PECAM-1

[1]Centro Nacional de Investigaciones Cardiovasculares (CNIC), 28029 Madrid, Spain. [2]University of Pennsylvania, Philadelphia, PA 19104, USA. [3]Instituto de Investigación Sanitaria Princesa. Universidad Autónoma de Madrid, 28006 Madrid, Spain. [4]FIRC Institute of Molecular Oncology, University of Milan, 20139 Milan, Italy. [5]Nagoya University, Nagoya, 464-8601, Japan.

*Author for correspondence (agarroyo@cnic.es)

Received 15 January 2014; Accepted 9 June 2014

Journal of Cell Science

Journal of Cell Science (2014) 127, 3768–3781 doi:10.1242/jcs.149518

in the continuous non-fenestrated endothelium of heart and lung vessels and in the specialized tight endothelium of the blood-brain barrier, but not in the continuous fenestrated endothelium of kidney glomeruli and spleen – a pattern indicating a correlation between EMMPRIN expression and junction strength (supplementary material Fig. S1A). In whole-mount specimens, EMMPRIN was also detected at the junctions of the microvasculature of the ear and at the endothelium of large vessels (aorta) (supplementary material Fig. S1B).

The enrichment of EMMPRIN at endothelial cell–cell junctions of different vascular beds suggests a function at these sites. We therefore analyzed the vasculature of EMMPRIN-deficient mice. EMMPRIN-null mice show no apparent vascular defect, and skin and organ coloration is similar to that of wild-type animals, indicating no hemorrhage or gross alterations to circulation. However, *ex vivo* whole-mount staining for the junction marker PECAM-1 revealed altered intercellular contacts in several vascular territories. In the microvasculature of the trachea and the ear, the cell-boundary PECAM-1 staining in EMMPRIN-deficient mice was diffuse and discontinuous compared with the sharp pattern observed in wild-type mice, especially at branch points, where the vessels also appeared to be dilated (Fig. 1A). A similar PECAM-1 phenotype was observed in the tracheal microvasculature of EMMPRIN-heterozygous mice, indicating that a wild-type amount of EMMPRIN is required for proper junction formation (data not shown). The pattern of PECAM-1 staining was also subtly irregular in straight large vessels of the ear and in aortas from EMMPRIN-null mice (Fig. 1A).

EMMPRIN-null mice do not display macroscopic edema, and skin-tone recovery after pressure application was comparable to that of wild-type animals; moreover, histological skin sections showed no signs of edema. Nonetheless, given the altered endothelial junction structure in EMMPRIN-null mice, we directly explored vessel integrity *in vivo* by injecting animals with Evans Blue. We observed greater accumulation of Evans Blue in the inflamed ears (after application of mustard oil) of EMMPRIN-null mice than in their wild-type counterparts (Fig. 1B); Evans Blue leakage in the inflamed ear was also significantly higher than normal in EMMPRIN heterozygous mice (data not shown). As a complementary approach, we monitored the tissue leakage of fluorescently labeled low- or high-molecular-mass dextran (4 kDa or 70 kDa) by confocal microscopy. Leakage of both dextrans was higher in the ears of EMMPRIN-null mice when compared with that of wild-type ears, both under basal conditions and upon inflammation induced by aural application of mustard oil (Fig. 1C).

EMMPRIN knockdown impairs the stability of adherens junctions

Confocal analysis confirmed that EMMPRIN is also located at junctions formed by human umbilical vein endothelial cells (HUVECs), where it partially colocalizes with the junction components VE-cadherin (48% colocalization), PECAM-1 (95%) and JAM-A (also known as F11R; 81%) (data not shown). We next investigated how adherens junctions were affected by EMMPRIN deficiency in human endothelial cells. siRNA-mediated knockdown of EMMPRIN expression with two independent oligonucleotides efficiently decreased protein expression for up to 72 h in culture (Fig. 2A). Immunostaining for endothelial junction components in EMMPRIN-silenced HUVECs revealed a marked alteration in the VE-cadherin pattern. In non-transfected (control) cells or cells transfected with a non-specific siRNA (Neg), VE-cadherin displayed a well-defined pattern of sharp contours at endothelial cell–cell contacts; by contrast, a broader, more irregular pattern was detected at most contacts between EMMPRIN-silenced cells (Fig. 2B). Image

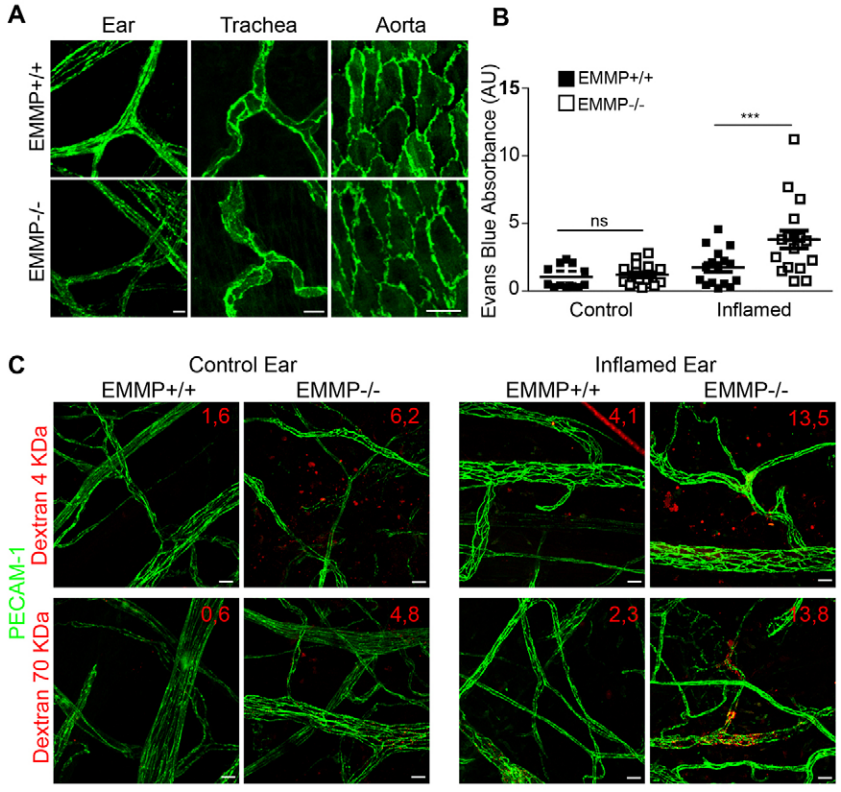

Fig. 1. EMMPRIN-deficient mice show altered endothelial junctions and increased microvascular permeability. (A) Representative images of whole-mount staining in wild-type (EMMP+/+) and EMMPRIN-null (EMMP−/−) mice for the junction marker PECAM-1 (green) in the trachea, ear and aorta. Scale bars: 20 μm. (B) Quantification of the tissue content of Evans Blue in mustard-oil-inflamed and mineral-oil-treated control ears from wild-type and EMMPRIN-deficient mice. AU, arbitrary units. Data show the mean±s.e.m. (four independent experiments; a total of 16 mice per genotype); ***$P<0.0001$; ns, non-significant (unpaired Student's *t*-test). (C) Representative merged images of PECAM-1 staining (green) in the microvasculature of control and mustard-oil-inflamed ears of wild-type and EMMPRIN-null mice 30 min after intravenous injection of 4-kDa or 70-kDa dextran–TRITC (red). Numbers in the upper-right corners show quantification of red fluorescence intensity. Scale bars: 20 μm.

Journal of Cell Science (2014) 127, 3768–3781 doi:10.1242/jcs.149518

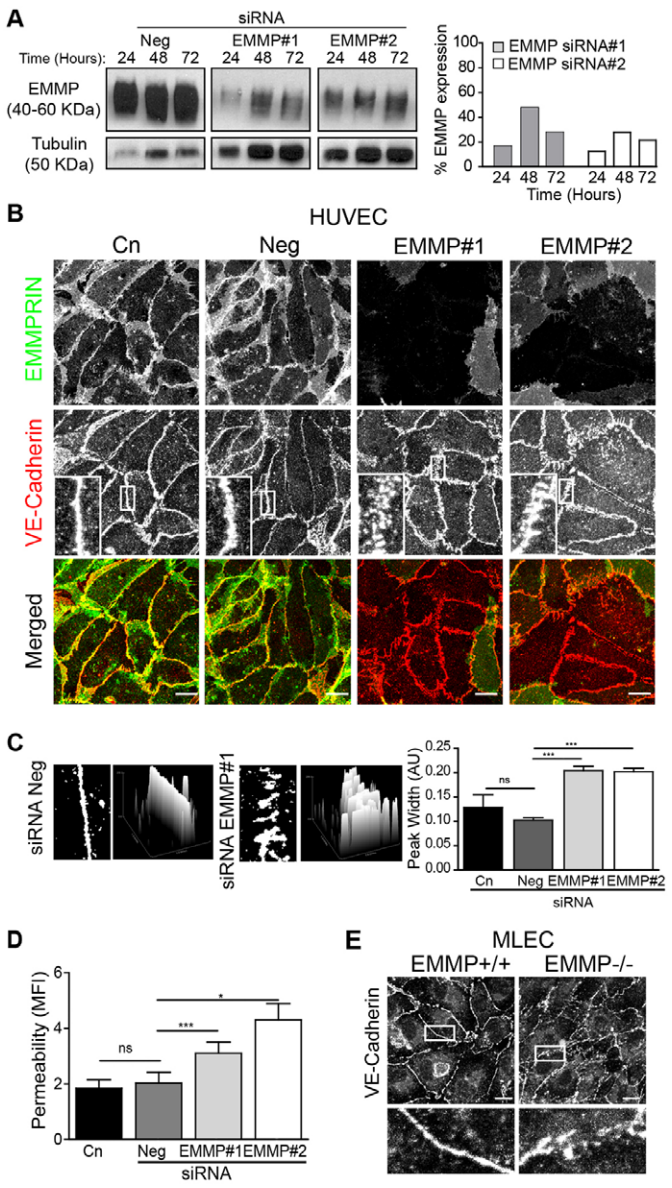

Fig. 2. VE-cadherin-containing junctions are impaired in human and mouse EMMPRIN-deficient endothelial cells. (A) Representative western blots of EMMPRIN protein levels in HUVECs transfected with control siRNA (Neg) or EMMPRIN-specific siRNAs (EMMP#1 or EMMP#2) up to 106 h post-transfection (equivalent to 72 h after seeding for monolayer formation). The chart on the right shows the efficiency of EMMPRIN silencing (the percentage of protein expression compared with that of the Neg siRNA sample at each time-point). Tubulin is shown as a loading control. (B) Representative black and white images of immunostaining for VE-cadherin (red in merge) and EMMPRIN (green in merge) in HUVECs transfected with negative-control siRNA or EMMPRIN-specific siRNAs. Control (Cn) indicates non-transfected HUVECs. Insets show magnified views of the boxed areas, with details of the VE-cadherin staining pattern at junctions. Scale bars: 20 μm. (C) Representative image analysis profiles of VE-cadherin staining performed as in B. Data show the mean±s.e.m. of the breadth of VE-cadherin staining at junctions (n=35 junctions quantified from three independent experiments per condition); ***P<0.0001; ns, non-significant. (D) EMMPRIN knockdown increases endothelial monolayer permeability *in vitro*. HUVECs transfected as indicated were grown to confluence on transwell filters and dextran–FITC was added to the upper chamber. Data show the mean±s.e.m. of the amount of labeled dextran recovered in the lower chamber after 1 h (n=3); *P<0.05; ***P<0.0001. (E) Representative black and white images of staining for VE-cadherin in MLECs from wild-type and EMMPRIN-null mice. Magnified views of the boxed areas are shown in the lower panel. Scale bars: 20 μm.

analysis confirmed a significantly wider peak of VE-cadherin intensity at the borders of EMMPRIN-knockdown cells (Fig. 2C). A similarly broadened distribution was observed for the VE-cadherin partner β-catenin (data not shown). These structural alterations resulted in impaired barrier function, as shown by the significantly higher permeability of EMMPRIN-knockdown HUVEC monolayers to labeled dextran in transwell assays (Fig. 2D). The function of EMMPRIN in endothelial cell–cell junctions was independently demonstrated in EMMPRIN-deficient primary mouse lung endothelial cells (MLECs), which also displayed a VE-cadherin distribution of reduced intensity, lower definition and an overall broadened pattern at cell–cell junctions (Fig. 2E; supplementary material Fig. S2E,F).

EMMPRIN regulates actomyosin-dependent contractility and forces at endothelial junctions

VE-cadherin stability of adherens junctions is related to the tension exerted by circumferential actin bundles together with NM-II at these sites (Hoelzle and Svitkina, 2012; Liu et al., 2010). We first observed that EMMPRIN colocalized with F-actin (as visualized by phalloidin staining) at filopodia and lamellipodia in both early exploratory immature cell–cell contacts (1 h) and mature junctions established over 48 h (Fig. 3A). The previously reported pattern of the actin network at immature endothelial junctions (Hoelzle and Svitkina, 2012) was detected at junctions formed by control endothelial cells after 1 h, whereas junctions in EMMPRIN-knockdown cells lacked this actin pattern at this early stage and were characterized by the persistence of radial actin filaments (Fig. 3B). To visualize the impact of EMMPRIN deficiency on live actin polymerization during both the formation and maturation of cell–cell contacts, we first knocked down EMMPRIN in human endothelial cells, transfected them with LifeAct and then stained them with a directly labeled anti-EMMPRIN antibody. Time-lapse video microscopy revealed colocalization of polymerized actin and EMMPRIN clusters at membrane contacts established by non-knockdown endothelial cells (Fig. 3C; supplementary material Movie 1). In these cells, actin transited from a network with few filaments perpendicular to the junction (see also Fig. 3B) to a pattern of parallel filaments as described previously (Mège et al., 2006). By contrast, in EMMPRIN-knockdown cells, the actin filaments mostly remained perpendicular to the junction (see also Fig. 3B) until the end of the sequence (8:20 h of time-lapse video microscopy, at 24 h after seeding (Fig. 3C; supplementary material Movie 2).

To further define actomyosin activity at endothelial junctions, we quantified active NM-II (by staining the phosphorylated regulatory myosin light chain; pMLC) and polymerized F-actin (by phalloidin staining) at cellular regions of interest defined around the junctions (ROIs; see Fig. 4A,B and Materials and Methods for details). EMMPRIN-knockdown human endothelial cells displayed reduced actomyosin activity at the junctions, as shown by the significantly decreased staining of pMLC and F-actin, contrasting with the punctate staining of pMLC and the enrichment of F-actin observed at the junctions of control cells (Fig. 4A,C). This reduction was further demonstrated by the significant decrease in the pMLC:MLC ratio observed by western blotting in membrane-enriched fractions from EMMPRIN-knockdown human endothelial cells compared with that of controls (Fig. 4D). Moreover, a similar reduction in pMLC and

Journal of Cell Science (2014) 127, 3768–3781 doi:10.1242/jcs.149518

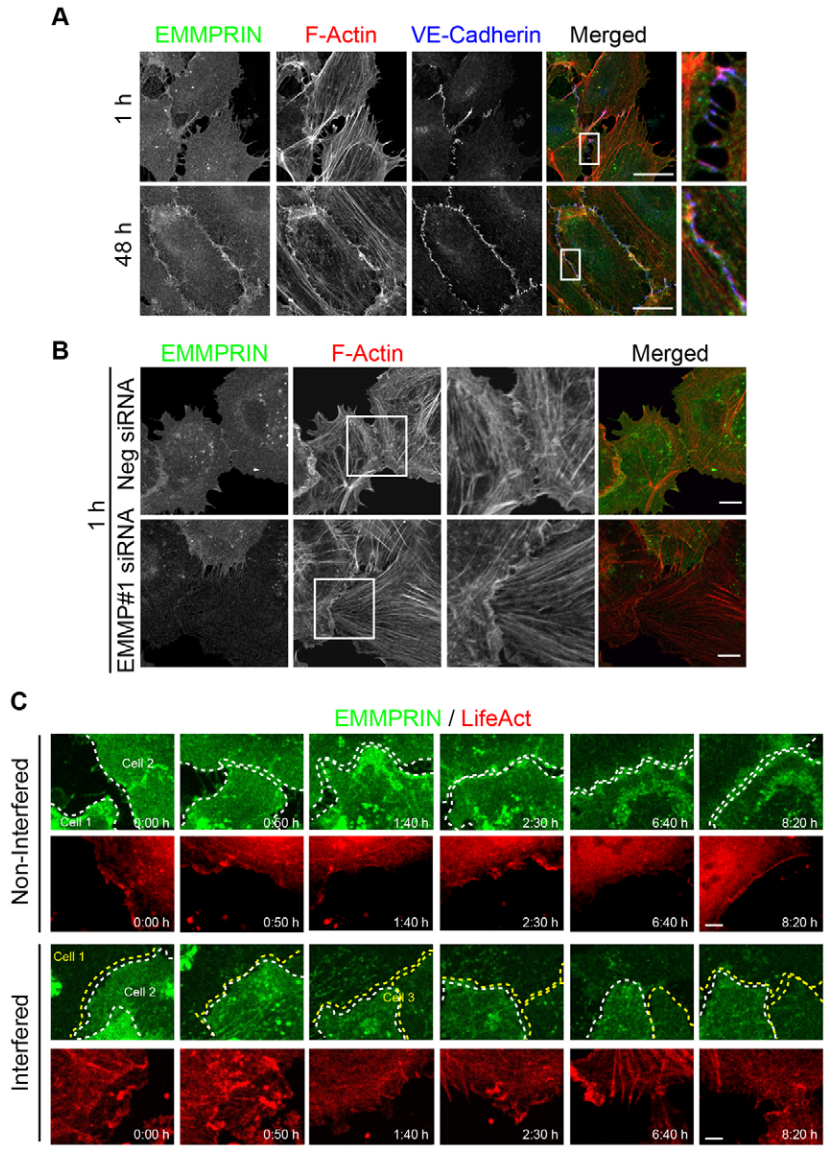

Fig. 3. EMMPRIN is required for actin organization at endothelial junctions. (A) Representative black and white images of staining for EMMPRIN (green in merge), F-actin (phalloidin; red in merge) and VE-cadherin (blue in merge) in HUVECs at 1 h and 48 h after seeding. Magnified views of the boxed areas (right) show colocalization of EMMPRIN with F-actin at early and mature endothelial cell–cell contacts. Scale bars: 20 μm. (B) Representative black and white images of staining for EMMPRIN (green in merge) and F-actin (red in merge) in control and EMMPRIN-knockdown HUVECs at 1 h after seeding. The boxed areas are shown in the magnified views; note the presence of a complex network of F-actin in control cells in contrast to the F-actin filaments in EMMPRIN-knockdown cells, which are perpendicular to the junction (particularly in the lower-right cell). Neg, cells transfected with control siRNA. Scale bars: 10 μm. (C) EMMPRIN-knockdown HUVECs were transfected with LifeAct (red) and stained with directly labeled anti-EMMPRIN mAb (green). Starting at 6 h after seeding, time-lapse images were recorded over 18 h. Selected images at the indicated time-points are shown with identifying cell numbers, and junctions are shown as dotted lines in white (for non-knockdown cells) or yellow (for EMMPRIN-knockdown cells). Scale bars: 5 μm.

F-actin and, therefore, actomyosin activity was also found at the aortic endothelial junctions of EMMPRIN-null mice analyzed *ex vivo*; this reduction was better visualized in a three-dimensional-rendering reconstruction of pMLC and F-actin images (Fig. 4E,F). We next quantified the linearity index (defined as the ratio of junction length to the distance between vertices) introduced by Takeichi's group in epithelial cells as a read-out of actomyosin contractility (Otani et al., 2006); as shown in Fig. 4G, VE-cadherin-based linearity index was significantly increased in EMMPRIN-knockdown human endothelial cells compared with that of control cells, demonstrating reduced actomyosin contractility in the absence of EMMPRIN. To directly quantify the forces exerted by actomyosin at the endothelial junctions, we plated human endothelial cells on an array of fluorescently labeled elastomeric microneedles, which allowed quantification of intercellular tugging forces in pairs of cells (Cohen et al., 2013; Liu et al., 2010). In accordance with image analysis and western blot data (Fig. 4A–D) and to increased linearity index (Fig. 4G), the intensity of tugging forces (the force across the cell junction) was significantly lower in EMMPRIN-knockdown cells (Fig. 4H).

We also observed a significant increase in pMLC (but not F-actin) in the interior of EMMPRIN-deficient HUVECs and aortic endothelial cells (supplementary material Fig. S2A). In an attempt to rescue the phenotype through the reestablishment of tension at the junctions, we next analyzed the effect of relaxing the inner non-muscle myosin activity with the inhibitor of Rho kinase Y27632, which only reduces pMLC inside cells, leaving intact punctate pMLC staining at junctions (Smutny et al., 2010; Totsukawa et al., 2000). Y27632 restored the linear VE-cadherin pattern and restored permeability in EMMPRIN-knockdown HUVECs to a level similar to that of control cells (supplementary material Fig. S2B–D); the inhibitor also restored the junction pattern and integrity in EMMPRIN-null MLECs (supplementary material Fig. S2E,F).

EMMPRIN associates with γ-catenin at endothelial junctions

The above results indicate that EMMPRIN contributes to pMLC regulation and actomyosin contractility at endothelial cell junctions either through direct interaction with the actomyosin machinery or through an adapter protein. To explore this, we used

Journal of Cell Science (2014) 127, 3768–3781 doi:10.1242/jcs.149518

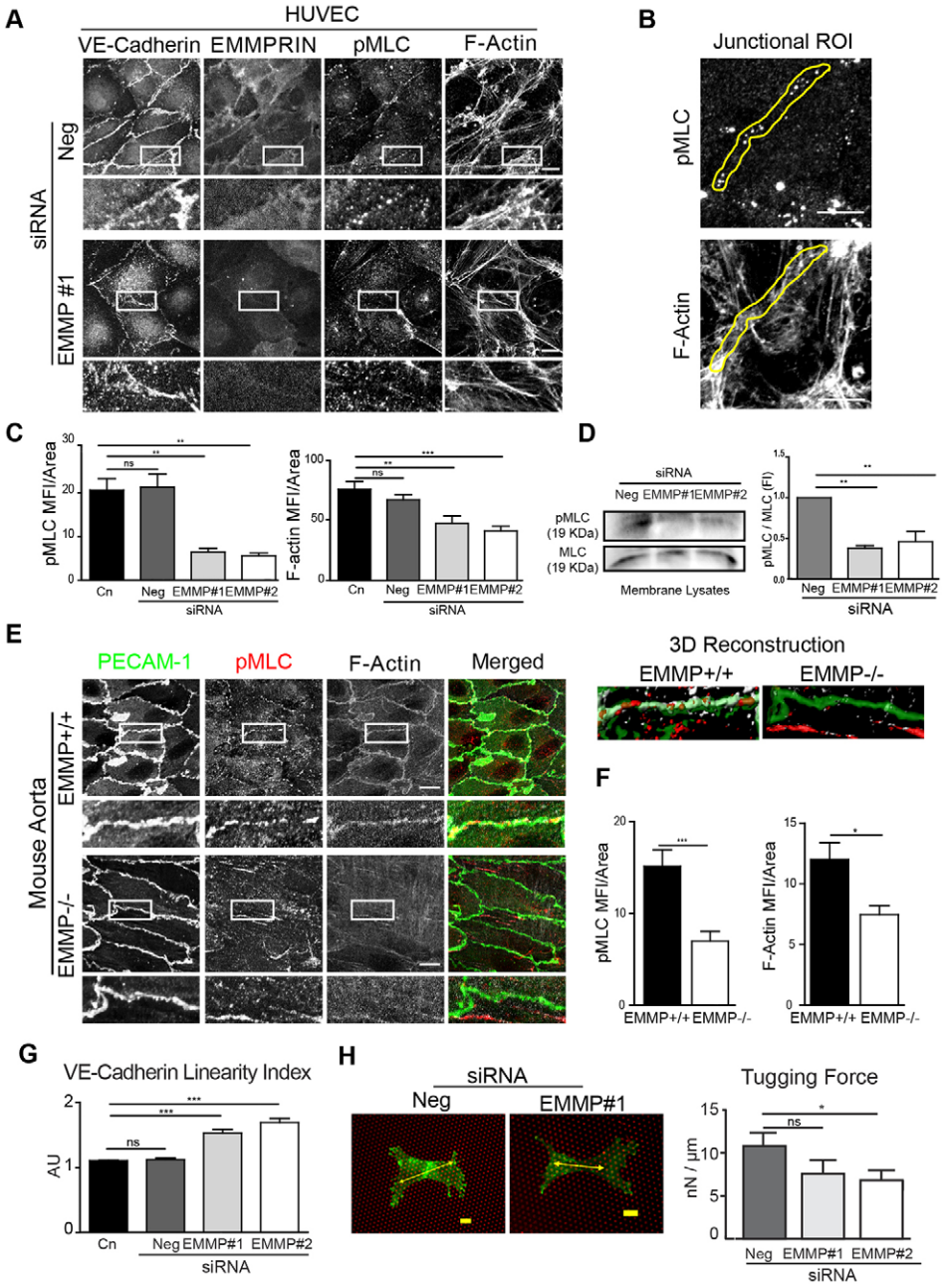

Fig. 4. EMMPRIN regulates actomyosin contractility and tugging forces at endothelial junctions. (A) Representative black and white images of VE-cadherin, EMMPRIN, pMLC and F-actin staining in control (Neg) and EMMPRIN-knockdown (EMMP#1) HUVECs. Boxed regions are shown in the magnified views below the images. Scale bars: 20 µm. (B) Junctional ROIs (outlined in yellow) were drawn as an area with a maximum width of 1.5–2 µm surrounding the junction (identified by VE-cadherin staining). Scale bars: 20 µm. (C) Quantification of mean fluorescence intensity (MFI) for pMLC and F-actin at junctions of control and EMMPRIN-knockdown HUVECs. Cn, non-transfected control. Data show the mean±s.e.m. (n=30–40 junctions quantified in two or three independent experiments per condition); **P<0.01; ***P<0.001; ns, non-significant. (D) Left, representative western blot of pMLC and MLC protein levels in membrane-enriched fractions isolated from control-siRNA-transfected and EMMPRIN-knockdown human endothelial cells. Right, graph shows the fold induction (FI, mean±s.e.m.) of pMLC:MLC ratios in EMMPRIN-knockdown versus control cells (n=3 independent experiments); **P<0.01. (E) Similar images and image analysis to that shown in A, performed in aortas of wild-type and EMMPRIN-null mice, showing junction staining with antibodies against PECAM-1 (green in merge) and pMLC (red in merge), and F-actin (white in merge) staining (left). Scale bars: 20 µm. Right, three-dimensional reconstruction from images of endothelial junctions from wild-type or EMMPRIN-deficient aortas was performed with Imaris software. Volumes were partially transparent to allow visualization of all the components of the junction. (F) Quantification of mean fluorescence intensity for pMLC and F-actin (phalloidin) at junctions of wild-type and EMMPRIN-deficient aortas. Data show the mean±s.e.m. (n=30–40 junctions were quantified from two or three independent experiments per condition); *P<0.05; ***P<0.001. (G) Linearity index was quantified with ImageJ software as the ratio of the length of VE-cadherin junction staining and the distance between junction vertices in non-transfected, control-siRNA-transfected and EMMPRIN-knockdown human endothelial cells. Data show the mean±s.e.m. (n=40–50 junctions per condition in three independent experiments); ***P<0.0001. (H) Tugging forces were quantified in EMMPRIN-siRNA-transfected HUVECs plated on elastomer plates coated with fibronectin (red) and immunostained for EMMPRIN (green). Representative images with the force vectors (yellow arrows) are shown on the left (vector scale bars: 50 nN). The graph showing the average of tugging forces for each condition is shown on the right. Data show the mean±s.e.m.; n=14, 8, 14 for negative siRNA, siRNA#1 and siRNA#2, respectively.

Journal of Cell Science (2014) 127, 3768–3781 doi:10.1242/jcs.149518

the EMMPRIN cytosolic tail as bait to search for interacting proteins in epithelial cell lysates. Mass spectrometry of pulled-down proteins identified several candidates, including γ-catenin, a known component of endothelial cell junctions. The association of EMMPRIN with γ-catenin in HUVECs was confirmed by co-immunoprecipitation (Fig. 5A). The immunoprecipitates did not contain VE-cadherin, and γ-catenin colocalized with EMMPRIN in VE-cadherin-null mouse endothelial cells, pointing to the VE-cadherin independence of this complex (Fig. 5B). EMMPRIN colocalized with γ-catenin at both early exploratory and stable junctions formed by human endothelial cells (Fig. 5C; data not shown). Moreover, γ-catenin was barely detected by immunostaining in EMMPRIN-knockdown endothelial cells, particularly at endothelial junctions, despite a lack of significant difference in γ-catenin protein levels as determined by western blotting, suggesting that EMMPRIN is necessary for the proper recruitment of γ-catenin to these sites (Fig. 5C,D). Levels of γ-catenin were also low at cell–cell junctions of the ear vessels from EMMPRIN-null mice, indicating that EMMPRIN contributes to γ-catenin recruitment to endothelial junctions *in vivo* (Fig. 5E). Microscopy analysis showed that siRNA-mediated knockdown of γ-catenin in human endothelial cells significantly decreased the amount of pMLC and F-actin at junctions, in a manner similar to that of EMMPRIN-knockdown cells, confirming the contribution of this complex to pMLC–actomyosin contractility at junctions (Fig. 5F,G).

An EMMPRIN–γ-catenin–Nm23 complex regulates actomyosin contractility at endothelial cell junctions through local ATP production

Given that actomyosin contractility requires ATP, we next investigated the possible role at the junction of the reported γ-catenin partner nucleoside diphosphate kinase Nm23 (Aktary et al., 2010), which is able to generate ATP by exchanging phosphate groups from NTP to ADP. The presence of Nm23 in the EMMPRIN molecular complex was confirmed by co-immunoprecipitation from endothelial cell lysates (Fig. 6A). In addition, although Nm23 staining was mostly diffuse within endothelial cells, Nm23 colocalized with EMMPRIN and γ-catenin at specific points in some junctions of confluent human endothelial cells (Fig. 6B); this was better visualized after methanol fixation or saponin treatment to remove the soluble cytosolic pool of Nm23 (supplementary material Fig. S3A). The interaction of EMMPRIN with γ-catenin and Nm23 was further demonstrated by using the proximity ligation assay (PLA), which showed positive signal for EMMPRIN–γ-catenin and for γ-catenin–Nm23 at the endothelial cell junctions of confluent HUVEC monolayers (Fig. 6B, lower panels). Moreover, Nm23 localization at endothelial cell junctions was significantly reduced in both EMMPRIN-knockdown and γ-catenin-knockdown HUVECs (Fig. 6C,D), pointing to an essential requirement for EMMPRIN–γ-catenin in Nm23 recruitment to the junctions. To better address this point, we transfected EMMPRIN-knockdown HUVECs with a myristoylated EMMPRIN cytosolic tail; we first confirmed that the myristoylated EMMPRIN cytosolic tail was recruited to endothelial cell junctions, likely due to cytosolic residues involved in EMMPRIN trafficking (Fig. 7A,B; Deora et al., 2004). The myristoylated EMMPRIN cytosolic tail rescued the presence of γ-catenin and Nm23 as well as pMLC and F-actin staining at the junctions of EMMPRIN-knockdown cells (Fig. 7A,B), indicating that the sole cytosolic EMMPRIN tail anchored to the membrane is able to recruit γ-catenin and Nm23, and that this interaction is essential for proper actomyosin contractility at junctions.

In order to gain further mechanistic insights, we next analyzed the impact of decreasing Nm23 levels on endothelial junction stability. Endothelial cell junctions were disrupted in Nm23-knockdown human endothelial cells, as indicated by decreased levels of pMLC and altered F-actin at junctions, resulting in a significantly increased linearity index together with reduced VE-cadherin staining and enhanced endothelial permeability (Fig. 8A–C; supplementary material Fig. S3B,C). Because Nm23 can directly regulate cytoskeleton contractility in *Dictyostelium* by providing ATP to the myosin molecule (Aguado-Velasco et al., 1996), we explored the possible involvement of this mechanism in mammalian endothelial cells by quantifying ATP production at endothelial junctions. We first used the Perceval plasmid to visualize and quantify ATP:ADP ratios (Berg et al., 2009) at endothelial junctions in the presence of inhibitors of the main sources of ATP production in endothelial cells (glycolysis and mitochondria; see Materials and Methods for details). We visualized and quantified ATP:ADP ratios before and after inhibitor treatment and observed that the ATP:ADP ratio at the endothelial cell periphery (junctional area) was decreased to a greater extent in EMMPRIN-knockdown compared with control knockdown endothelial cells upon inhibitor addition, pointing to lower production of ATP in the absence of EMMPRIN at the membrane (Fig. 8D). To assess this, we directly quantified ATP production in membrane-enriched fractions in the presence of inhibitors of ATPase synthase and adenylate kinase and in the presence of GTP and ADP as substrates for Nm23. ATP production in these conditions was lower in membranes from EMMPRIN-knockdown cells than in membranes from control knockdown cells (Fig. 8E). Moreover, an inhibitory anti-Nm23 antibody significantly decreased ATP production by membranes from control human endothelial cells but had only a minor effect in EMMPRIN-knockdown cells, indicating that Nm23 makes an essential contribution to ATP production at the membrane in the presence of EMMPRIN (Fig. 8E). Overall these findings point to decreased pMLC and actomyosin contractility and impaired junctions in EMMPRIN-deficient endothelial cells as a result of defective local ATP production.

DISCUSSION

Our results show that EMMPRIN is essential for endothelial junction stability and vascular integrity. EMMPRIN, through a newly identified association with γ-catenin and Nm23 during junction formation, acts as a key intermediary between the plasma membrane and actomyosin contractility by providing ATP, thus coordinating the forces required for junction initiation, stabilization and integrity *in vitro* and *in vivo* (supplementary material Fig. S4).

Endothelial cell–cell adhesions are essential for vascular integrity, and their alteration results in severe disorders (Dejana et al., 2009). Despite a lack of previous vascular phenotype described in EMMPRIN-null mice (Muramatsu and Miyauchi, 2003), we observe that they show above-normal vascular leakage under basal and inflammatory conditions, demonstrating an essential contribution of EMMPRIN to endothelial barrier functioning *in vivo*. This permeability phenotype is unlike that of mice deficient for other Ig family members present at endothelial junctions, such as PECAM-1 or JAM-C (also known as JAM-3) (Graesser et al., 2002; Orlova et al., 2006),

Journal of Cell Science (2014) 127, 3768–3781 doi:10.1242/jcs.149518

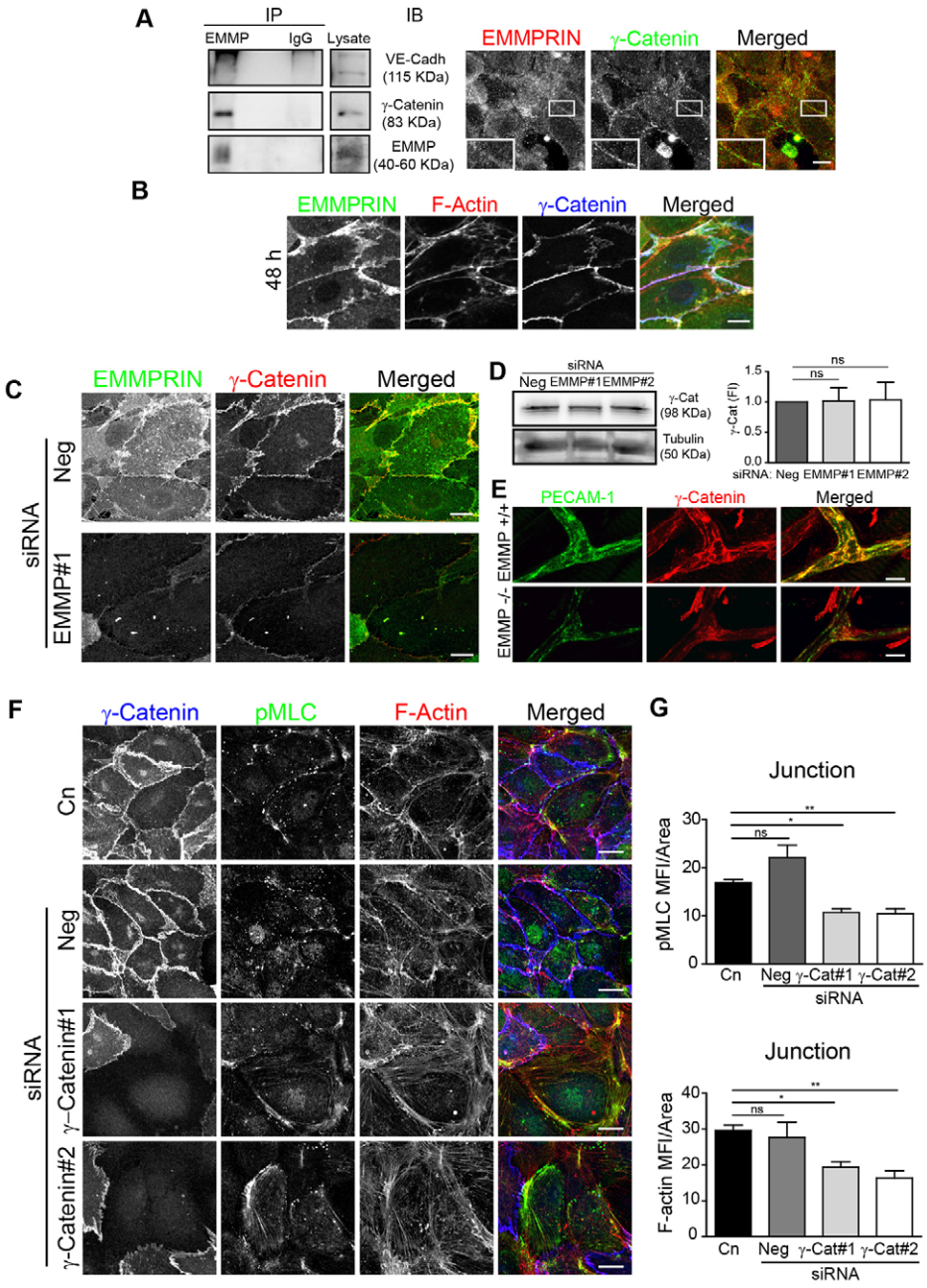

Fig. 5. EMMPRIN interacts with γ-catenin at endothelial cell junctions. (A) Left, representative western blot (IB) analysis for γ-catenin and VE-cadherin in EMMPRIN immunoprecipitates (IP) from HUVECs. Right, representative black and white images of immunofluorescence staining for EMMPRIN (red in merge) and γ-catenin (green in merge) in VE-cadherin-null mouse endothelial cells; insets show details of the staining pattern at junctions from the boxed areas. Scale bar: 10 μm. (B) Representative confocal fluorescence images of EMMPRIN (green in merge), F-actin (phalloidin; red in merge) and γ-catenin (blue in merge) in HUVECs, showing colocalization of EMMPRIN and γ-catenin at 48 h after seeding. Scale bar: 10 μm. (C) Representative black and white confocal immunofluorescence images of staining for EMMPRIN (green in merge) and γ-catenin (red in merge) in control-siRNA-transfected (Neg) and EMMPRIN-knockdown (EMMP#1) HUVECs at 48 h after seeding. Scale bars: 10 μm. (D) Left, representative western blot of γ-catenin protein levels in RIPA lysates from control-siRNA-transfected and EMMPRIN-knockdown cells; right, graph shows the fold induction (FI) of γ-catenin in EMMPRIN-knockdown versus control cells. Data show the mean±s.e.m. (three independent experiments); ns, non-significant. (E) Representative images showing whole-mount staining of PECAM-1 (green) and γ-catenin (red) in the ears of wild-type and EMMPRIN-null mice. Scale bars: 20 μm. (F) Representative black and white images of staining for γ-catenin (blue in merge), pMLC (green in merge) and F-actin (phalloidin; red in merge) in non-transfected control (Cn), control-siRNA-transfected and γ-catenin-knockdown HUVECs. Scale bars: 20 μm. (G) Quantification of mean fluorescence intensities (MFI) for pMLC and F-actin at junctions of control versus γ-catenin-knockdown HUVECs. Data show the mean±s.e.m. (n=30–40 junctions were quantified in two or three independent experiments per condition); *P<0.05; **P<0.01.

suggesting that each junction component has selective and specific functions in the regulation of vessel integrity. Because permeability differences in arteries, capillaries and venules correlate with the heterogeneous actin organization and function in these vascular beds (Prasain and Stevens, 2009), it is also possible that EMMPRIN contributes to this heterogeneity through

Journal of Cell Science (2014) 127, 3768–3781 doi:10.1242/jcs.149518

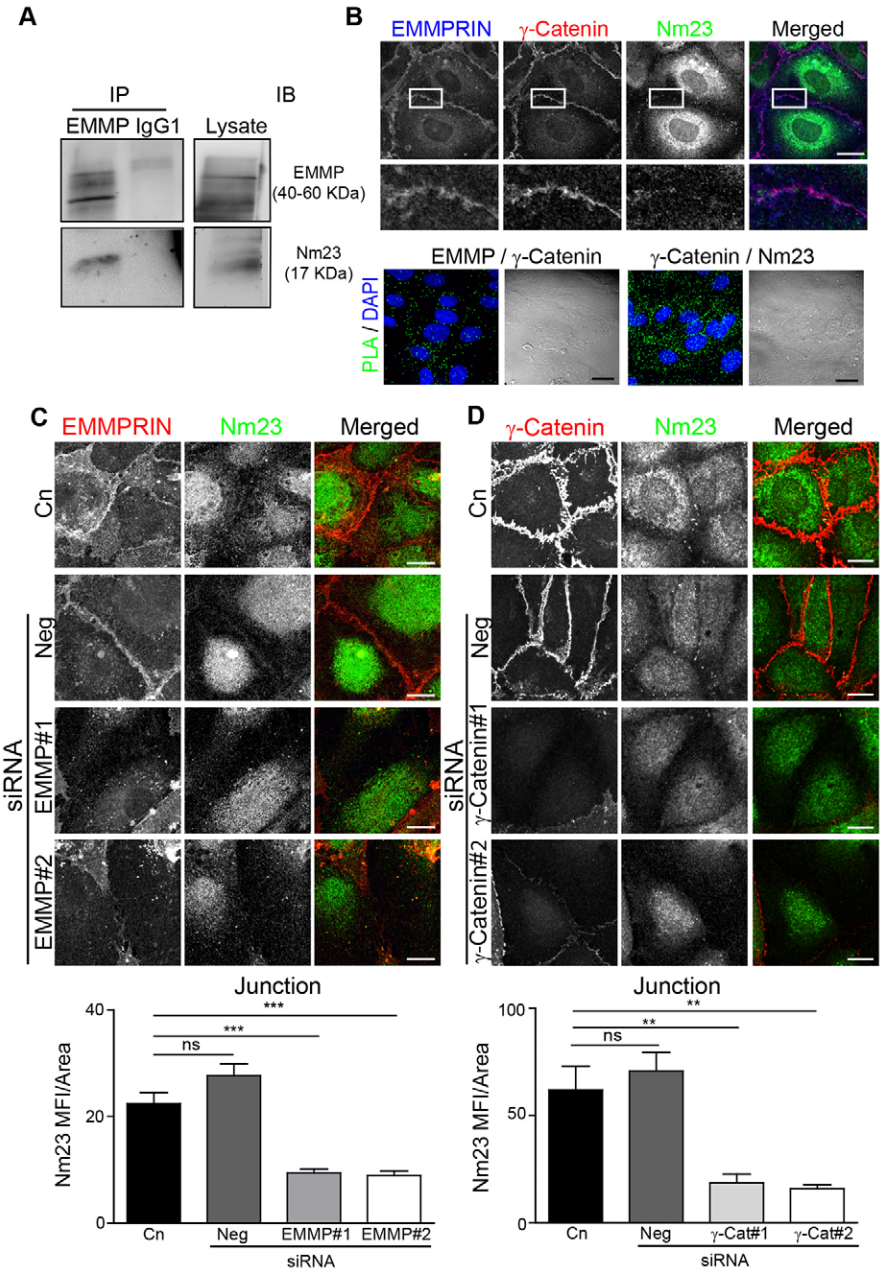

Fig. 6. Nm23 is associated with the EMMPRIN–γ-catenin complex at endothelial junctions. (A) Representative western blot analysis for Nm23 in EMMPRIN immunoprecipitates (IP) from HUVECs. (B) Upper panels, representative black and white confocal fluorescence images of staining for EMMPRIN (blue in merge), γ-catenin (red in merge) and Nm23 (green in merge) in HUVECs at 48 h after seeding. Magnified views of the boxed areas are shown below the main images. Lower panels, representative brightfield and merged images of DAPI (blue) and proximity ligation assay (PLA, green) for EMMPRIN and γ-catenin (left) and for γ-catenin and Nm23 (right) in HUVECs fixed with methanol. Scale bars: 20 µm. (C) Upper panels, representative black and white confocal fluorescence images of EMMPRIN (red in merge) and Nm23 (green in merge) in non-transfected control (Cn), control-siRNA-transfected (Neg) and EMMPRIN-knockdown HUVECs at 48 h after seeding. Lower panel, quantification of mean fluorescence intensity (MFI) for Nm23 at the junctions of control and EMMPRIN-knockdown HUVECs. Data show the mean±s.e.m. (30–40 junctions were quantified in three independent experiments per condition); ***$P<0.001$; ns, non-significant. (D) Upper panel, representative black and white confocal images of the staining of γ-catenin (red in merge) and Nm23 (green in merge) in control and γ-catenin-knockdown HUVECs. Lower panel, quantification of mean fluorescence intensity for Nm23 at the junctions of control and γ-catenin-knockdown HUVECs. Data show the mean±s.e.m. ($n=30$–40 junctions were quantified in two independent experiments per condition); **$P<0.01$. Scale bars: 20 µm.

its preferential expression at the junctions of certain vascular beds, in particular at those with a tighter endothelial barrier.

Forces generated at cell–cell junctions through dynamic interactions between transmembrane proteins and the actomyosin cytoskeleton are especially important for the maintenance of endothelial barrier fitness, but the underlying molecular mechanisms were not fully understood. Here, we identify EMMPRIN as an essential coordinator of these forces because, in its absence, actomyosin-driven contractility is reduced and VE-cadherin contacts are not properly established; in this regard, we have extended the utility and complementarity (to the quantification of junctional pMLC and F-actin by image analysis) of the linearity index as a read-out of actomyosin contractility not only in epithelial but also in endothelial junctions (Otani et al., 2006) Direct quantification by elastomer sensors (Liu et al., 2010) revealed that forces across cell–cell junctions (tugging forces) are significantly diminished in EMMPRIN-knockdown endothelial cells. Because this method only allows force quantification in endothelial cell pairs it will be of interest to use alternative approaches, such as the recently established fluorescence resonance energy transfer (FRET)-based tension sensors to quantify junctional forces in established endothelial monolayers (Conway et al., 2013). The relevance of balanced forces for endothelial junction integrity is further supported by the restoration of the wild-type junction phenotype in EMMPRIN-deficient cells upon relaxation of inward tension with a Rho kinase inhibitor.

This function of EMMPRIN in orchestrating spatiotemporal junctional actomyosin (pMLC and F-actin) contractility is particularly relevant, because this network is just beginning to be elucidated in endothelial cells (Ando et al., 2013; Huveneers et al., 2012; Wimmer et al., 2012). EMMPRIN absence resulted in delayed actin maturation at endothelial junctions, in accordance with its role in organizing cortical actin at neuromuscular junctions in *Drosophila* (Besse et al., 2007). In terms of the mechanism

Journal of Cell Science (2014) 127, 3768–3781 doi:10.1242/jcs.149518

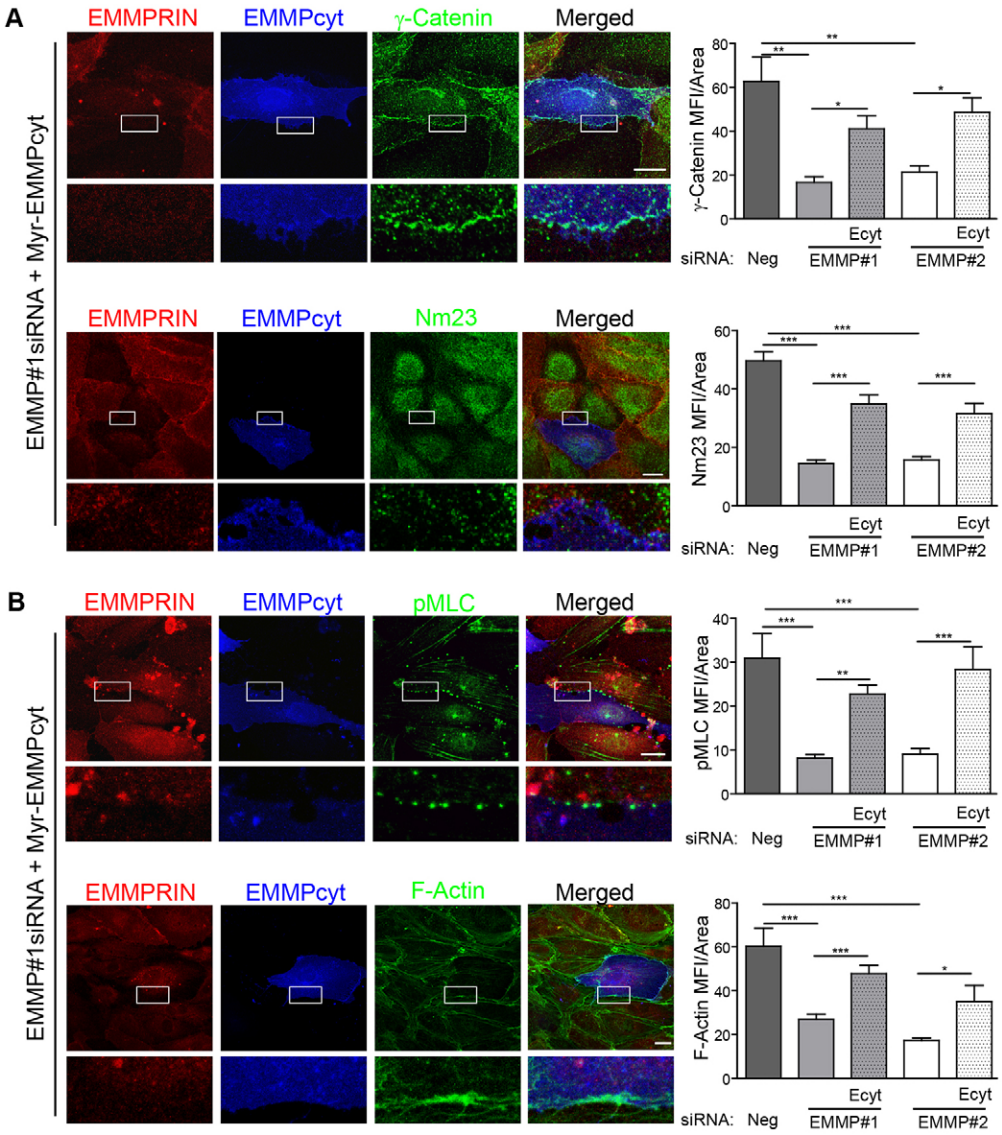

Fig. 7. The EMMPRIN cytosolic tail mediates γ-catenin and Nm23 recruitment and actomyosin contractility at endothelial junctions. Representative images are shown of EMMPRIN (red), γ-catenin (green) or Nm23 (green) (A) and of EMMPRIN (red), pMLC (green) or F-actin (phalloidin; green) (B) in EMMPRIN-knockdown HUVECs (EMMP#1 and EMMP#2) transfected with a GFP-tagged myristoylated EMMPRIN cytosolic tail construct (EMMPcyt; blue). Boxed areas are shown at a higher magnification below the main images. Graphs on the right show the quantification of mean fluorescence intensity (MFI) for γ-catenin and Nm23 (A) or pMLC and F-actin (B) at the junctions of cells transfected with siRNA against EMMPRIN, either with or without the GFP–myr-EMMPRIN cytosolic tail. Neg, control-siRNA-transfected cells. Data show the mean±s.e.m. (30–50 junctions were analyzed in two independent experiments per group); *$P<0.05$; **$P<0.01$; ***$P<0.001$. Scale bars: 20 μm.

involved, the polybasic juxtamembrane region of EMMPRIN is important for cortical actin organization in *Drosophila*, but no EMMPRIN cytosolic interactions have been described, except for an association with the microtubule protein Hook1 that was reported recently (Besse et al., 2007; Maldonado-Báez et al., 2013). We have identified by mass spectrometry a novel molecular interaction of the cytosolic tail of EMMPRIN with γ-catenin, with this complex being required for proper actomyosin-dependent forces during the formation of endothelial junctions (data not shown). This is in line with the specific role of γ-catenin in organizing the cortical actin skeleton described in *Xenopus* (Kofron et al., 2002). Because γ-catenin can also associate with CPI-17 (also known as PPP1R14A), an inhibitor of MLC phosphatase, this might contribute to the overall regulation of MLC phosphorylation at the junction (Kim et al., 2013), supporting broader effects of γ-catenin on junctional F-actin and on adherens junctions.

The identification of the EMMPRIN–γ-catenin complex raises the question of how it regulates actomyosin contractility and junction stability. ATP is required for phosphorylation of MLC by MLCK, and we therefore explored the possible role of Nm23, a member of the nucleoside diphosphate kinase (NDPK) family, which was recently identified as a partner of γ-catenin in tumor cells (Aktary et al., 2010). Nm23 could be found at endothelial junctions together with EMMPRIN and γ-catenin, and knockdown of either of these proteins resulted in a significant decrease in Nm23 localization to these sites. A myristoylated EMMPRIN cytosolic tail rescued γ-catenin and Nm23 presence at junctions, together with pMLC and F-actin organization at these sites, further supporting an

Journal of Cell Science (2014) 127, 3768–3781 doi:10.1242/jcs.149518

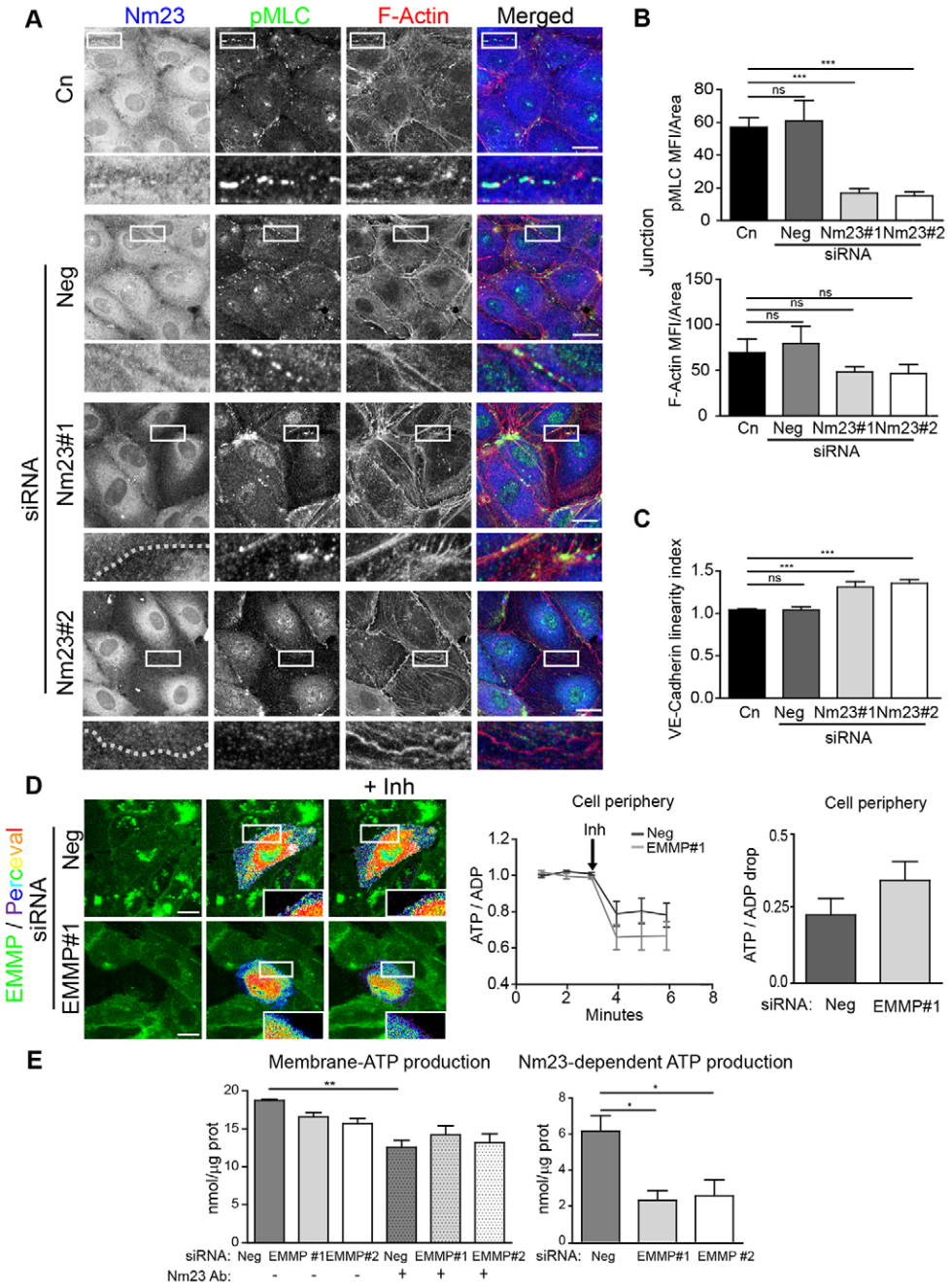

Fig. 8. The presence of Nm23 at endothelial junctions is required for MLC phosphorylation and ATP production at these sites. (A) Representative black and white images of staining for Nm23 (blue in merge), pMLC (green in merge) and F-actin (phalloidin; red in merge) and the merged images are shown in non-transfected control (Cn), control-siRNA-transfected (Neg) and Nm23-knockdown (Nm23#1 and Nm23#2) HUVECs. Boxed regions are shown in the magnified views below the images; dotted lines mark the junction in Nm23-knockdown cells. Scale bars: 20 µm. (B) Quantification of mean fluorescence intensities (MFI) for pMLC and F-actin at junctions of control versus Nm23-knockdown HUVECs. Data show the mean±s.e.m. (n=15 junctions were quantified in two independent experiments per condition); ***P<0.001; ns, non-significant. (C) Quantification of VE-cadherin linearity index in control versus Nm23-knockdown HUVECs. Data show the mean±s.e.m. (n=20–30 junctions were quantified per condition in two independent experiments); ***P<0.0001. (D) Left, representative images of human endothelial cells stained for EMMPRIN and visualized for Perceval fluorescent signal (ATP:ADP ratio shown in pseudo-color scale) in the absence or presence of metabolic inhibitors (Inh) in control-siRNA-transfected and EMMPRIN-knockdown (EMMP#1) endothelial cells. Scale bars: 20 µm. Middle, ATP:ADP ratios quantified in the cell periphery (junctional area) are plotted for the time scale over which pH was stable (around 3 min before and after the addition of inhibitors). Data show the mean±s.e.m. Right, graph shows the relative drop in the ATP:ADP ratio after inhibitor treatment, normalizing basal levels to 1. Data show the mean±s.e.m. (n=6 cells analyzed for each condition). (E) ATP production in cell membranes from control and EMMPRIN-knockdown HUVECs (n=3). Graphs show ATP generated by enzymatic reaction after the addition of reaction buffer in the absence or presence of the inhibitory antibody (Ab) anti-Nm23; Nm23-dependent ATP production was calculated from the difference in ATP levels produced in the presence or absence of the antibody. Data show the mean±s.e.m.; *P<0.05, **P<0.01.

essential contribution of the EMMPRIN–γ-catenin–Nm23 complex to the regulation of tension at junctions. A detailed analysis of how this molecular complex is assembled and the protein domains involved in the interactions deserves further investigation.

However, the mechanism by which Nm23 might regulate endothelial intercellular adhesion remained unclear. The primary function of NDPK is to provide phosphates to ADP, thus generating ATP, which could then be used for myosin-dependent cytoskeleton contraction, as reported in *Dictyostelium* (Gajewski et al., 2003). By using (for the first time in endothelial cells) the recently developed Perceval tool (Berg et al., 2009; Zala et al., 2013), we could visualize and quantify ATP:ADP ratios at the subcellular level and show that, in inhibitor-treated cells, the absence of EMMPRIN resulted in lower ATP:ADP ratios at the junctional area compared with those of control cells. The requirement for EMMPRIN at the endothelial membrane in the process of local ATP production was further confirmed in isolated membranes; in addition, the ability of an inhibitory anti-Nm23 antibody to mimic the effect of EMMPRIN depletion, significantly reducing ATP production in membranes, further demonstrates the contribution of Nm23 to ATP production within the EMMPRIN–γ-catenin complex at human endothelial junctions. The EMMPRIN–γ-catenin–Nm23 complex would provide a local source of ATP required for MLCK-dependent MLC phosphorylation and actomyosin-driven forces at junctions; alternatively, local ATP can be crucial for the dynamic regulation of weak/strong actomyosin force cycles required for efficient contractility (Aprodu et al., 2008). This Nm23/NDPK function would be particularly important when ATP levels are low (Aguado-Velasco et al., 1996), as might be the case at maturing junctions, where the packed actin cytoskeleton might restrict free diffusion of ATP from the cytosol. Nm23 knockdown resulted, however, in a more severe junction phenotype than that observed in EMMPRIN-knockdown or γ-catenin-knockdown endothelial cells, because, in addition to decreased junctional pMLC and increased linearity index and to altered VE-cadherin pattern and augmented monolayer permeability, endothelial cells displayed lamellipodia-like protrusions at the cell–cell adhesions, resembling disrupted junctions. This might be related to global cellular effects of Nm23 knockdown and to additional functions attributed to Nm23 in regulating adherens junctions, such as Rab5-mediated endocytosis and inhibition of Rac signaling by sequestering Rac guanine nucleotide exchange factors (GEFs) in *Drosophila*, and Arf6-dependent E-cadherin endocytosis in canine epithelial cells (Palacios et al., 2002; Woolworth et al., 2009). The EMMPRIN–γ-catenin–Nm23 complex reveals an unexpected link between compartmentalized energy production and endothelial cell junction stability that might be relevant to situations in which changes in endothelial cell metabolism and junction remodeling need to be coordinated, such as during angiogenesis, collective migration and tissue morphogenesis.

MATERIALS AND METHODS

Mice

EMMPRIN-deficient mice were generated as described previously (Muramatsu and Miyauchi, 2003). EMMPRIN heterozygotes were crossed following the strategy described previously (Chen et al., 2004), and null littermates were used for experiments. Mice were kept in the CNIC Animal Facility under pathogen-free conditions and according to institutional guidelines. All animal studies were approved by the CNIC Animal Care Ethical Committee.

Antibodies and reagents

Mouse monoclonal antibody (mAb) VJ1/9.1 against the EMMPRIN ectodomain was generated in the laboratory of F.S.-M. The anti-VE-cadherin TEA1/31 and anti-PECAM-1 TP1/15 mAbs have been described previously (Yáñez-Mó et al., 1998). The anti-JAM-A BV16 mAb was obtained from Hycult Biotech. Rabbit anti-phospho-myosin light chain (pMLC) antibody was from Cell Signaling, rabbit anti-myosin light chain was from Santa Cruz and phalloidin–Texas-Red was obtained from BD Pharmingen. Whole-mount mouse vessels were stained with anti-PECAM-1 from Millipore, anti-VE-cadherin and anti-γ-catenin from BD Biosciences, and anti-EMMPRIN from eBiosciences. Goat anti-mouse-IgG, anti-armenian-hamster-IgG and anti-rat-IgG secondary antibodies were from Jackson ImmunoResearch. Type-I collagen was purchased from PureCol, Opti-MEM from Gibco, Medium 199 from Lonza, Evans Blue from Sigma and Oligofectamine and dextran–TRITC from Invitrogen. The Rho kinase inhibitor Y27632 was obtained from Sigma. Anti-Nm23 antibodies were purchased from Santa Cruz Biotechnology and GeneTex. LifeAct (Riedl et al., 2008) and myristoylated cytosolic EMMPRIN (Ruiz et al., 2008) constructs were provided by Roland Wedlich-Soldner and Xosé Bustelo, respectively.

Whole-mount staining

Mice were perfused with 1% paraformaldehyde (PFA) in PBS. Postnatal retinas and the trachea, aorta and ears of adult animals were extracted and post-fixed in 1% PFA for 1 h at room temperature. Tissues were then incubated with primary antibodies in 5% goat serum (Jackson ImmunoResearch) overnight at room temperature. Samples were washed for 8 h in PBS containing 0.3% Triton X-100 and labeled with the appropriate secondary antibody overnight at room temperature. The next day, samples were washed again in PBS containing 0.3% Triton X-100 and mounted in Vectashield (Vector Laboratories). Samples were examined with a Leica TCS Sp5 spectral confocal microscope or a Zeiss LSM 700 confocal microscope.

In vivo permeability assay

A modified Miles assay was used to examine vessel permeability in 4–8-week-old anesthetized mice (Miles and Miles, 1952). Briefly, the mice were injected intravenously with 100 µl of 5 mg/ml dextran–TRITC (4 KDa or 70 KDa) or 100 µl of Evans Blue to a final concentration of 30 mg/kg and, after 5 min, 5% mustard oil in mineral oil (Sigma) was applied to the right ear. Mineral oil alone was applied to the left ear as a negative control. After 30 min, mice were sacrificed, and ears from dextran-injected mice were extracted and processed for whole-mount staining and ears from Evans-Blue-injected mice were dried and weighed. Evans Blue was extracted from tissues in formamide (Fluka) and measured in a spectrophotometer (BioRad).

Cell culture

Human umbilical vein endothelial cells (HUVECs) were obtained and cultured as described previously (Yáñez-Mó et al., 1998). Cells from passages two to four were used in all assays. For endothelial monolayer formation assay, HUVECs were seeded at subconfluence on collagen-I-coated plates or coverslips. Cells were processed for analysis at 1, 24, 48 and 72 h after seeding. Mouse lung endothelial cells (MLECs) were obtained and cultured as described previously (Oblander et al., 2005). Briefly, lungs from wild-type or EMMPRIN-null mice were excised, disaggregated and digested in 0.1% collagenase (Gibco) for 1 h at 37℃. The cell suspensions were seeded onto plates coated with 10 µg/ml fibronectin (Sigma), 10 µg/ml collagen I (PureCol) and 0.1% gelatin (Sigma). After attachment, cells were negatively selected with anti-CD16/CD32 mAb (BD Biosciences) coupled to magnetic beads (Dynal, Invitrogen), and then positively selected with anti-ICAM-2 (BD Biosciences) coupled to magnetic beads. Cells were seeded onto plates coated with 10 µg/ml collagen I before assays.

Immunofluorescence microscopy

Tissue cryosections were fixed with 4% PFA, 2% sucrose in PBS for 15 min and quenched for 1 h at room temperature with 100 mM glycine in PBS. After washing, sections were blocked overnight with 2% bovine serum albumin (BSA) and 5% goat serum in PBS. Sections were then incubated with primary antibodies for 2–3 h at 37℃. After washes,

samples were incubated with goat secondary antibodies for 1 h at 37℃, washed again and mounted with Prolong (Invitrogen). Cells were grown on collagen-I-coated coverslips and samples were fixed at different times in 4% PFA, 2% sucrose in PBS for 15 min at room temperature. Samples were blocked with 2% BSA and, when necessary, permeabilized with 0.1% Triton X-100 for 10 min. For colocalization of Nm23 with EMMPRIN and γ-catenin, cells were also fixed in methanol at −20℃ for 2 min or treated with 0.01% saponin for 5 min at room temperature before PFA fixation. Coverslips were incubated with the primary antibody for 1 h at 37℃ and, after washes, labeled with the appropriate secondary antibody under the same conditions. For double staining of EMMPRIN and other molecules using mouse antibodies, immunofluorescence was performed as described above and coverslips were incubated with anti-EMMPRIN (VJ1/9.1) directly labeled with Alexa Fluor 488 or Alexa Fluor 594 (Zenon, Molecular Probes).

Proximity ligation assay

Human endothelial cells were fixed with methanol at −20℃ for 2 min and stained with rabbit antibody against EMMPRIN C-terminus (GTX62657, Genetex) and mouse anti-γ-catenin or with mouse anti-γ-catenin and rabbit anti-Nm23. PLA was performed following the manufacturer's instructions (Duolink *In Situ* kit, Olink Biosciences). Briefly, samples were blocked with the blocking solution for 30 min at 37℃ and incubated overnight with the primary antibodies at 4℃. The following day, the samples were washed and incubated for 1 h at 37℃ with PLA probes for rabbit and mouse antibodies. After washing, samples were incubated with the ligase for 30 min at 37℃, washed again and incubated with the polymerase for 100 min at 37℃. Finally, the samples were washed, dried completely and mounted in Duolink *In Situ* Mounting Medium with DAPI.

siRNA-mediated interference and transfections

HUVECs (3×10^5) were seeded onto collagen-I-coated six-well plates the day before siRNA transfection. The next morning, two independent EMMPRIN siRNA oligonucleotides or negative siRNA (Ambion) were mixed with 4 µl of Oligofectamine (Invitrogen) in 400 µl of Opti-MEM and added to the cells (final concentration of 100 nM). After 4 h, 600 µl of Opti-MEM containing 30% FBS was added, and the cells were incubated overnight at 37℃. Most experiments were performed with both siRNAs, but for some experiments the results are shown for siRNA#1 only. This siRNA decreases EMMPRIN expression less efficiently than siRNA#2, but in a higher percentage of cells. Transfection of HUVECs with γ-catenin or Nm23 siRNA oligonucleotides (Ambion) followed a similar protocol. For the expression of LifeAct or the myristoylated cytosolic tail of EMMPRIN, cells were first transfected with siRNA as described and, the next day, were transfected with 2 µg of DNA in Lipofectamine 2000 (Invitrogen). Cells were analyzed at 24 h after transfection.

Time-lapse video microscopy experiments

After siRNA-mediated interference, HUVECs were transfected with LifeAct and seeded onto collagen-I-coated glass-bottomed plates. Before imaging, cells were stained with Zenon Alexa-Fluor-488-labeled anti-EMMPRIN antibody (VJ1/9.1; Molecular Probes) for 30 min at room temperature. For time-lapse video microscopy, cells were maintained at 37℃ under 5% CO_2, and *Z*-stacks of eight confocal sections (1.2 µM) were taken every 5 min with a Zeiss LSM 700 microscope for 20 h.

Image acquisition and analysis

Images were acquired with 40×/1.25 or 63×/1.4 objectives on an Sp5 confocal microscope (Leica Microsystems) or with 40×/1.3 or 63×/1.4 objectives on a LSM700 confocal microscope (Carl Zeiss). Images were converted to TIFF files with LAS AF (Leica Microsystems) or ZEN (Carl Zeiss) software, respectively, and brightness and contrast were adjusted with Photoshop CS3. The colocalization of EMMPRIN with other junction proteins was analyzed with LAS AF software. Data are presented as the percentage of colocalization measured in ROIs surrounding the junction. Junctional ROIs were drawn as an area with a maximum width of 1.5–2 µm surrounding the junction. The VE-cadherin fluorescence staining pattern was quantified with ImageJ, making plot profiles within similar ROIs as in colocalization analysis. In each of three independent experiments, four to six junctions were analyzed per field in an average of five fields. Fluorescence intensities for γ-catenin, Nm23, pMLC and F-actin were also analyzed with ImageJ. Mean intensity per pixel was measured in junctional ROIs and in the rest of the cell (interior). Linearity index, defined as the ratio of junction length to the distance between vertices by Takeichi's group (Otani et al., 2006), was quantified by using ImageJ software based on VE-cadherin staining of endothelial cell junction length.

In vitro permeability assay

HUVEC monolayer permeability was measured with the Millipore *In Vitro* Permeability Assay kit. Briefly, 120,000 cells were seeded onto the membranes of the chambers provided with the kit. After 48 h, dextran–FITC was added to the upper chamber and was recovered at different time-points from the lower chamber and measured in a fluorimeter (Fluoroskan Ascent, Thermo Scientific).

Tugging forces

Polydimethylsiloxane (PDMS) microneedle array substrates were fabricated as described previously (Fu et al., 2010). Bowtie patterns had a total area of 1600 μm^2. To measure forces exerted at the junctions, control HUVECs (Neg) or EMMPRIN-knockdown cells (siRNA#1 and siRNA#2) were plated over elastomer sensors with fibronectin micropatterning, fixed with 4% PFA in PBS for 15 min and stained for EMMPRIN. Tugging forces were measured as described previously (Liu et al., 2010). Briefly, microneedle deflections were calculated using Matlab to determine the displacement of the centroid of the microneedle at the tip. Forces were then computed from the known spring constant of the microneedle (7.2 nN/µm). Cells exist in a quasi-static equilibrium where the net force sums to zero (Balaban et al., 2001; Tan et al., 2003). The intercellular tugging force is therefore equal in magnitude and opposite in direction to the measured net traction force reported by the microneedle array (Cohen et al., 2013; Liu et al., 2010).

Co-immunoprecipitation and western blotting

Cells were lysed in RIPA buffer for 5 min at 4℃ and scraped. Lysates were cleared by spinning at 20,000 ***g***, 4℃ for 15 min, and 5× Laemmli buffer was added to the supernatant. Cell proteins were resolved by SDS-PAGE and transferred to nitrocellulose membranes. Blots were blocked overnight at 4℃ in TBS-T containing 5% BSA and were incubated with primary and secondary antibodies in TBS-T for 1 h at room temperature. Signal on washed blots was detected by enhanced chemiluminescence (GE Healthcare Life Sciences). For pMLC and MLC detection, membranes from control-knockdown and EMMPRIN-knockdown human endothelial cells were isolated as detailed for ATP production assays below, and the blots were processed as described above. For co-immunoprecipitation, confluent cells were incubated for 1 h at 4℃ with VJ1/9.1 mAb or an IgG1 control (2 µg each per 3×10^6 cells). Cells were lysed and cleared as before, and the lysates were incubated with Protein-G–Sepharose (GE Healthcare Life Sciences) for 1 h at 4℃. Beads were washed six times with lysis buffer and the proteins were separated and immunodetected as above.

Perceval assay

After siRNA-mediated interference, HUVECs were transfected with Perceval plasmid (Addgene) by the calcium phosphate method (Armesilla et al., 1999) and were analyzed in a Zeiss LSM 700 confocal microscope equipped with a 40× oil-immersion objective. For Perceval signal, excitation was set at 405 nm (ADP sensitive) and 488 nm (ATP sensitive) and detection of photomultiplier (PMT) was set at 500–560 nm (Berg et al., 2009; Zala et al., 2013). At 30 min before the experiment, human endothelial cells were stained with the directly labeled (Zenon) anti-EMMPRIN antibody to identify EMMPRIN-knockdown cells. Endothelial cells were equilibrated for 15 min before recording in the following buffer: 15 mM HEPES, 120 mM NaCl, 3 mM KCl, 2 mM $CaCl_2$, 1 mM $MgCl_2$, 1.25 mM Na_2HPO_4,

3 mM $NaHCO_3$, 5 mM glucose and 0.2 mM sodium pyruvate (pH 7.4). As a control for possible effects of pH variations on ATP:ADP signal, pH was registered by adding 5 µM SNARF 5 probe (Life Technologies) in complete medium for 25 min, 1 h before the experiment. For SNARF 5, excitation was set at 555 nm and detection was set at 575–595 nm (pH sensitive) and 610–647 nm (pH insensitive). pH and Perceval (ATP:ADP) signals were quantified by the ratio intensity of the two corresponding detection channels. To inhibit ATP production by mitochondria and glycolysis, human endothelial cells were treated with rotenone (1 µM), oligomycin (5 µM) and 2-deoxyglucose (20 mM) (all from Sigma-Aldrich). Cells were visualized, and ATP:ADP ratios were quantified over a time range spanning from before to after treatment with the combination of inhibitors for which no variations in pH were observed. Analysis of the intensity ratios was performed with ImageJ both at the cell periphery (equivalent to junctional ROI) and over the total cellular area.

Membrane fractioning and ATP production assay

Cells were washed and treated with ice-cold hypotonic lysis buffer (10 mM Tris-HCl pH 7.4, 1.5 mM $MgCl_2$, 5 mM KCl, 1 mM dithiothreitol, 0.2 mM sodium vanadate and protease inhibitors) for 5 min. Cell lysates were homogenized with 30 strokes of a Dounce homogenizer and homogenates were centrifuged at 1000 ***g*** for 3 min. The supernatants were then spun at 40,000 ***g*** for 30 min at 4℃ in a refrigerated centrifuge, and the crude membrane pellet was gently washed with hypotonic lysis buffer and resuspended in RIPA buffer. Membrane fractions were then assayed for total protein. ATP production by membrane-enriched fractions was measured by a kinetic luminescence assay (Vives-Bauza et al., 2007). Briefly, enriched membranes were diluted in buffer A (150 mM KCl, 25 mM Tris-HCl pH 7.4, 2 mM EDTA, 0.1% BSA, 10 mM KPO_4, 0.1 mM $MgCl_2$) in the presence of 150 µM ADP, 150 µM GTP, 1 µM oligomycin and 150 µM diadenosine pentaphosphate. To inhibit the reaction, anti-Nm23 antibody (Santa Cruz Biotechnology) was added at a final dilution of 1:100.

Statistical analysis

Student's *t*-test was used for statistical comparisons of two groups of data. For three or more groups assuming Gaussian distribution, one-way ANOVA with Dunnet's multiple comparisons post-test was used for comparisons with controls, and Newman-Keuls test was used for comparisons between different groups of data.

Acknowledgements

We thank Roland Wedlich-Soldner [Institute of Cell Dynamics and Imaging (Max Plank), Münster, Germany] for LifeAct, Xosé Bustelo (Centro de Investigación del Cáncer, Salamanca, Spain) for myr-EMMPRIN cytosolic constructs and Simon Bartlett (Centro Nacional de Investigaciones Cardiovasculares, Madrid, Spain) for English editing.

Competing interests

The authors declare no competing interests.

Author contributions

V.M. designed experiments, performed research and wrote the paper; P.G., A.P. and R.A.-P. performed research; J.G.-E. performed Perceval assays; M.Y.-M. performed proteomics analysis; O.B. and K.K. contributed reagents and analytical tools; F.O. contributed experimental techniques; M.B. and C.C. performed elastomer sensor experiments; J.A.E., E.D. and F.S.M. contributed techniques or reagents and discussion; and A.G.A. designed the research and wrote the paper.

Funding

This work was supported by grants from Fundación Ramón Areces; and Ministerio de Economía y Competitividad [grant numbers RD12/0042/0023 and SAF2011-25619 to A.G.A, RD12/0042/0056 to F.S.-M. (RD grants are cofunded by FEDER)]; from the European Research Council [grant number ERC-2011AdG 294340 GENTRIS to F.S.-M.]; from the Associazione Italiana per la Ricerca sul Cancro; and European Research Council to E.D.; and grants from the National Institutes of Health; the RESBIO Technology Resource for Polymeric Biomaterials; and the Penn Nano/Bio Interface Center to C.C. V.M. was funded by the Comunidad Autónoma de Madrid [grant number S2010/BMD-2312 Angiobodies 2.0]. The Centro Nacional de Investigaciones Cardiovasculares (CNIC) is supported by the Ministerio de Economía y Competitividad and the Pro-CNIC Foundation. Deposited in PMC for release after 12 months.

Supplementary material

Supplementary material available online at
http://jcs.biologists.org/lookup/suppl/doi:10.1242/jcs.149518/-/DC1

References

Abraham, S., Yeo, M., Montero-Balaguer, M., Paterson, H., Dejana, E., Marshall, C. J. and Mavria, G. (2009). VE-Cadherin-mediated cell-cell interaction suppresses sprouting via signaling to MLC2 phosphorylation. *Curr. Biol.* **19**, 668-674.

Aguado-Velasco, C., Véron, M., Rambow, J. A. and Kuczmarski, E. R. (1996). NDP kinase can modulate contraction of Dictyostelium cytoskeletons. *Cell Motil. Cytoskeleton* **34**, 194-205.

Aktary, Z., Chapman, K., Lam, L., Lo, A., Ji, C., Graham, K., Cook, L., Li, L., Mackey, J. R. and Pasdar, M. (2010). Plakoglobin interacts with and increases the protein levels of metastasis suppressor Nm23-H2 and regulates the expression of Nm23-H1. *Oncogene* **29**, 2118-2129.

Ando, K., Fukuhara, S., Moriya, T., Obara, Y., Nakahata, N. and Mochizuki, N. (2013). Rap1 potentiates endothelial cell junctions by spatially controlling myosin II activity and actin organization. *J. Cell Biol.* **202**, 901-916.

Aprodu, I., Redaelli, A. and Soncini, M. (2008). Actomyosin interaction: mechanical and energetic properties in different nucleotide binding states. *Int. J. Mol. Sci.* **9**, 1927-1943.

Armesilla, A. L., Lorenzo, E., Gómez del Arco, P., Martínez-Martínez, S., Alfranca, A. and Redondo, J. M. (1999). Vascular endothelial growth factor activates nuclear factor of activated T cells in human endothelial cells: a role for tissue factor gene expression. *Mol. Cell. Biol.* **19**, 2032-2043.

Balaban, N. Q., Schwarz, U. S., Riveline, D., Goichberg, P., Tzur, G., Sabanay, I., Mahalu, D., Safran, S., Bershadsky, A., Addadi, L. et al. (2001). Force and focal adhesion assembly: a close relationship studied using elastic micropatterned substrates. *Nat. Cell Biol.* **3**, 466-472.

Baum, B. and Georgiou, M. (2011). Dynamics of adherens junctions in epithelial establishment, maintenance, and remodeling. *J. Cell Biol.* **192**, 907-917.

Berditchevski, F., Chang, S., Bodorova, J. and Hemler, M. E. (1997). Generation of monoclonal antibodies to integrin-associated proteins. Evidence that alpha3beta1 complexes with EMMPRIN/basigin/OX47/M6. *J. Biol. Chem.* **272**, 29174-29180.

Berg, J., Hung, Y. P. and Yellen, G. (2009). A genetically encoded fluorescent reporter of ATP:ADP ratio. *Nat. Methods* **6**, 161-166.

Besse, F., Mertel, S., Kittel, R. J., Wichmann, C., Rasse, T. M., Sigrist, S. J. and Ephrussi, A. (2007). The Ig cell adhesion molecule Basigin controls compartmentalization and vesicle release at Drosophila melanogaster synapses. *J. Cell Biol.* **177**, 843-855.

Bougatef, F., Quemener, C., Kellouche, S., Naïmi, B., Podgorniak, M. P., Millot, G., Gabison, E. E., Calvo, F., Dosquet, C., Lebbé, C. et al. (2009). EMMPRIN promotes angiogenesis through hypoxia-inducible factor-2alpha-mediated regulation of soluble VEGF isoforms and their receptor VEGFR-2. *Blood* **114**, 5547-5556.

Chen, S., Kadomatsu, K., Kondo, M., Toyama, Y., Toshimori, K., Ueno, S., Miyake, Y. and Muramatsu, T. (2004). Effects of flanking genes on the phenotypes of mice deficient in basigin/CD147. *Biochem. Biophys. Res. Commun.* **324**, 147-153.

Chen, Y., Zhang, H., Gou, X., Horikawa, Y., Xing, J. and Chen, Z. (2009). Upregulation of HAb18G/CD147 in activated human umbilical vein endothelial cells enhances the angiogenesis. *Cancer Lett.* **278**, 113-121.

Cohen, D. M., Yang, M. T. and Chen, C. S. (2013). Measuring cell-cell tugging forces using bowtie-patterned mPADs (microarray post detectors). *Methods Mol. Biol.* **1066**, 157-168.

Conway, D. E., Breckenridge, M. T., Hinde, E., Gratton, E., Chen, C. S. and Schwartz, M. A. (2013). Fluid shear stress on endothelial cells modulates mechanical tension across VE-cadherin and PECAM-1. *Curr. Biol.* **23**, 1024-1030.

Dejana, E. (2004). Endothelial cell-cell junctions: happy together. *Nat. Rev. Mol. Cell Biol.* **5**, 261-270.

Dejana, E., Tournier-Lasserve, E. and Weinstein, B. M. (2009). The control of vascular integrity by endothelial cell junctions: molecular basis and pathological implications. *Dev. Cell* **16**, 209-221.

Deora, A. A., Gravotta, D., Kreitzer, G., Hu, J., Bok, D. and Rodriguez-Boulan, E. (2004). The basolateral targeting signal of CD147 (EMMPRIN) consists of a single leucine and is not recognized by retinal pigment epithelium. *Mol. Biol. Cell* **15**, 4148-4165.

Deora, A. A., Philp, N., Hu, J., Bok, D. and Rodriguez-Boulan, E. (2005). Mechanisms regulating tissue-specific polarity of monocarboxylate transporters and their chaperone CD147 in kidney and retinal epithelia. *Proc. Natl. Acad. Sci. USA* **102**, 16245-16250.

Fu, J., Wang, Y. K., Yang, M. T., Desai, R. A., Yu, X., Liu, Z. and Chen, C. S. (2010). Mechanical regulation of cell function with geometrically modulated elastomeric substrates. *Nat. Methods* **7**, 733-736.

Gajewski, C. D., Yang, L., Schon, E. A. and Manfredi, G. (2003). New insights into the bioenergetics of mitochondrial disorders using intracellular ATP reporters. *Mol. Biol. Cell* **14**, 3628-3635.

Giannotta, M., Trani, M. and Dejana, E. (2013). VE-cadherin and endothelial adherens junctions: active guardians of vascular integrity. *Dev. Cell* **26**, 441-454.
Graesser, D., Solowiej, A., Bruckner, M., Osterweil, E., Juedes, A., Davis, S., Ruddle, N. H., Engelhardt, B. and Madri, J. A. (2002). Altered vascular permeability and early onset of experimental autoimmune encephalomyelitis in PECAM-1-deficient mice. *J. Clin. Invest.* **109**, 383-392.
Hoelzle, M. K. and Svitkina, T. (2012). The cytoskeletal mechanisms of cell-cell junction formation in endothelial cells. *Mol. Biol. Cell* **23**, 310-323.
Huveneers, S., Oldenburg, J., Spanjaard, E., van der Krogt, G., Grigoriev, I., Akhmanova, A., Rehmann, H. and de Rooij, J. (2012). Vinculin associates with endothelial VE-cadherin junctions to control force-dependent remodeling. *J. Cell Biol.* **196**, 641-652.
Kim, K. M., Adyshev, D. M., Kása, A., Zemskov, E. A., Kolosova, I. A., Csortos, C. and Verin, A. D. (2013). Putative protein partners for the human CPI-17 protein revealed by bacterial two-hybrid screening. *Microvasc. Res.* **88**, 19-24.
Kofron, M., Heasman, J., Lang, S. A. and Wylie, C. C. (2002). Plakoglobin is required for maintenance of the cortical actin skeleton in early Xenopus embryos and for cdc42-mediated wound healing. *J. Cell Biol.* **158**, 695-708.
Liu, Z., Tan, J. L., Cohen, D. M., Yang, M. T., Sniadecki, N. J., Ruiz, S. A., Nelson, C. M. and Chen, C. S. (2010). Mechanical tugging force regulates the size of cell-cell junctions. *Proc. Natl. Acad. Sci. USA* **107**, 9944-9949.
Maldonado-Báez, L., Cole, N. B., Krämer, H. and Donaldson, J. G. (2013). Microtubule-dependent endosomal sorting of clathrin-independent cargo by Hook1. *J. Cell Biol.* **201**, 233-247.
Mège, R. M., Gavard, J. and Lambert, M. (2006). Regulation of cell-cell junctions by the cytoskeleton. *Curr. Opin. Cell Biol.* **18**, 541-548.
Miles, A. A. and Miles, E. M. (1952). Vascular reactions to histamine, histamine-liberator and leukotaxine in the skin of guinea-pigs. *J. Physiol.* **118**, 228-257.
Millimaggi, D., Mari, M., D'Ascenzo, S., Carosa, E., Jannini, E. A., Zucker, S., Carta, G., Pavan, A. and Dolo, V. (2007). Tumor vesicle-associated CD147 modulates the angiogenic capability of endothelial cells. *Neoplasia* **9**, 349-357.
Muramatsu, T. and Miyauchi, T. (2003). Basigin (CD147): a multifunctional transmembrane protein involved in reproduction, neural function, inflammation and tumor invasion. *Histol. Histopathol.* **18**, 981-987.
Oblander, S. A., Zhou, Z., Gálvez, B. G., Starcher, B., Shannon, J. M., Durbeej, M., Arroyo, A. G., Tryggvason, K. and Apte, S. S. (2005). Distinctive functions of membrane type 1 matrix-metalloprotease (MT1-MMP or MMP-14) in lung and submandibular gland development are independent of its role in pro-MMP-2 activation. *Dev. Biol.* **277**, 255-269.
Orlova, V. V., Economopoulou, M., Lupu, F., Santoso, S. and Chavakis, T. (2006). Junctional adhesion molecule-C regulates vascular endothelial permeability by modulating VE-cadherin-mediated cell-cell contacts. *J. Exp. Med.* **203**, 2703-2714.
Otani, T., Ichii, T., Aono, S. and Takeichi, M. (2006). Cdc42 GEF Tuba regulates the junctional configuration of simple epithelial cells. *J. Cell Biol.* **175**, 135-146.
Palacios, F., Schweitzer, J. K., Boshans, R. L. and D'Souza-Schorey, C. (2002). ARF6-GTP recruits Nm23-H1 to facilitate dynamin-mediated endocytosis during adherens junctions disassembly. *Nat. Cell Biol.* **4**, 929-936.
Prasain, N. and Stevens, T. (2009). The actin cytoskeleton in endothelial cell phenotypes. *Microvasc. Res.* **77**, 53-63.
Riedl, J., Crevenna, A. H., Kessenbrock, K., Yu, J. H., Neukirchen, D., Bista, M., Bradke, F., Jenne, D., Holak, T. A., Werb, Z. et al. (2008). Lifeact: a versatile marker to visualize F-actin. *Nat. Methods* **5**, 605-607.
Ruiz, S., Castro-Castro, A. and Bustelo, X. R. (2008). CD147 inhibits the nuclear factor of activated T-cells by impairing Vav1 and Rac1 downstream signaling. *J. Biol. Chem.* **283**, 5554-5566.
Schreiner, A., Ruonala, M., Jakob, V., Suthaus, J., Boles, E., Wouters, F. and Starzinski-Powitz, A. (2007). Junction protein shrew-1 influences cell invasion and interacts with invasion-promoting protein CD147. *Mol. Biol. Cell* **18**, 1272-1281.
Smutny, M., Cox, H. L., Leerberg, J. M., Kovacs, E. M., Conti, M. A., Ferguson, C., Hamilton, N. A., Parton, R. G., Adelstein, R. S. and Yap, A. S. (2010). Myosin II isoforms identify distinct functional modules that support integrity of the epithelial zonula adherens. *Nat. Cell Biol.* **12**, 696-702.
Tan, J. L., Tien, J., Pirone, D. M., Gray, D. S., Bhadriraju, K. and Chen, C. S. (2003). Cells lying on a bed of microneedles: an approach to isolate mechanical force. *Proc. Natl. Acad. Sci. USA* **100**, 1484-1489.
Tang, W. and Hemler, M. E. (2004). Caveolin-1 regulates matrix metalloproteinases-1 induction and CD147/EMMPRIN cell surface clustering. *J. Biol. Chem.* **279**, 11112-11118.
Totsukawa, G., Yamakita, Y., Yamashiro, S., Hartshorne, D. J., Sasaki, Y. and Matsumura, F. (2000). Distinct roles of ROCK (Rho-kinase) and MLCK in spatial regulation of MLC phosphorylation for assembly of stress fibers and focal adhesions in 3T3 fibroblasts. *J. Cell Biol.* **150**, 797-806.
Vives-Bauza, C., Yang, L. and Manfredi, G. (2007). Assay of mitochondrial ATP synthesis in animal cells and tissues. *Methods Cell Biol.* **80**, 155-171.
Wimmer, R., Cseh, B., Maier, B., Scherrer, K. and Baccarini, M. (2012). Angiogenic sprouting requires the fine tuning of endothelial cell cohesion by the Raf-1/Rok-α complex. *Dev. Cell* **22**, 158-171.
Woolworth, J. A., Nallamothu, G. and Hsu, T. (2009). The Drosophila metastasis suppressor gene Nm23 homolog, awd, regulates epithelial integrity during oogenesis. *Mol. Cell. Biol.* **29**, 4679-4690.
Xu, D. and Hemler, M. E. (2005). Metabolic activation-related CD147-CD98 complex. *Mol. Cell. Proteomics* **4**, 1061-1071.
Yáñez-Mó, M., Alfranca, A., Cabañas, C., Marazuela, M., Tejedor, R., Ursa, M. A., Ashman, L. K., de Landázuri, M. O. and Sánchez-Madrid, F. (1998). Regulation of endothelial cell motility by complexes of tetraspan molecules CD81/TAPA-1 and CD151/PETA-3 with alpha3 beta1 integrin localized at endothelial lateral junctions. *J. Cell Biol.* **141**, 791-804.
Zala, D., Hinckelmann, M. V., Yu, H., Lyra da Cunha, M. M., Liot, G., Cordelières, F. P., Marco, S. and Saudou, F. (2013). Vesicular glycolysis provides on-board energy for fast axonal transport. *Cell* **152**, 479-491.

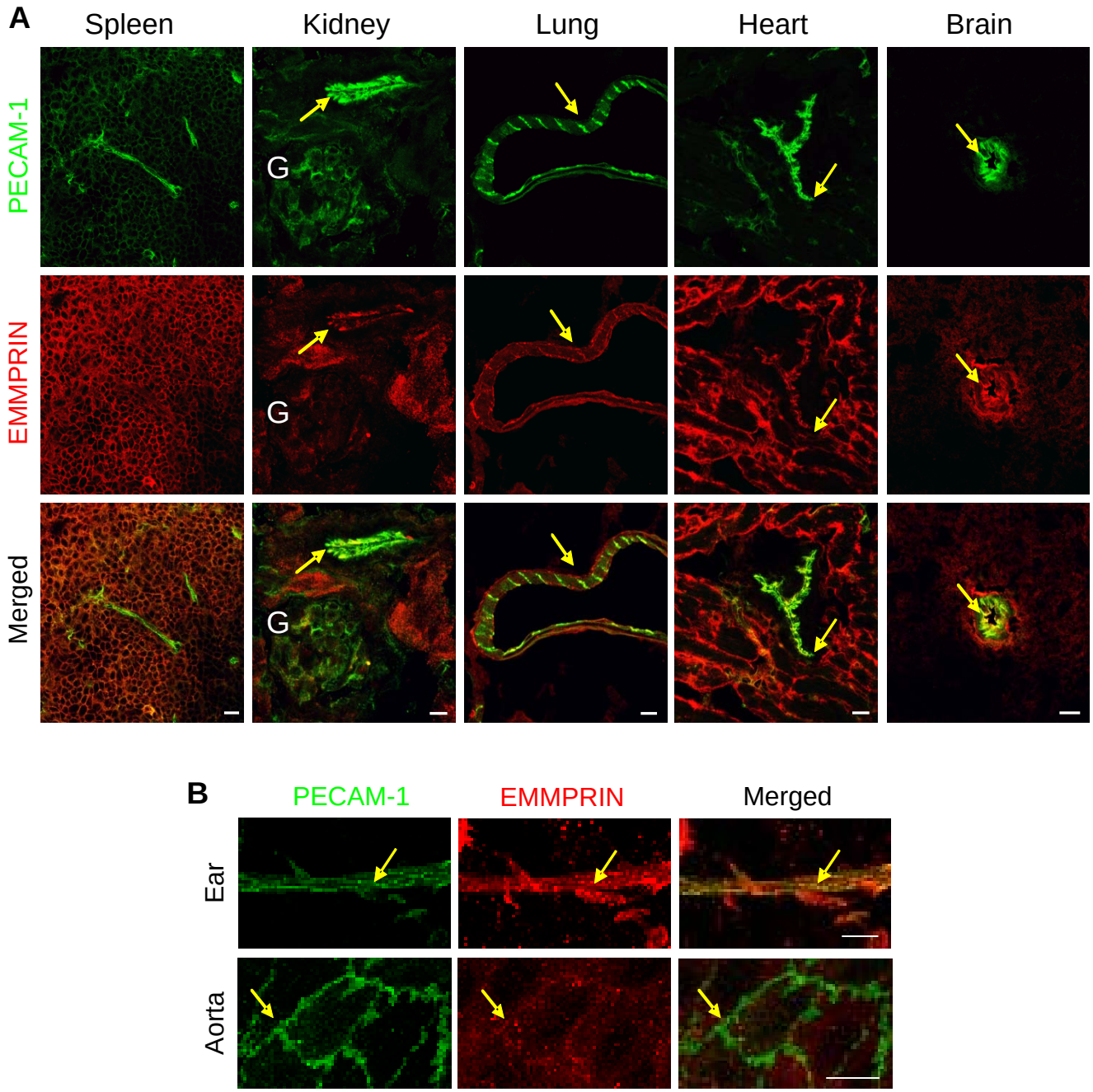

Fig. S1. EMMPRIN is located at endothelial cell junctions in specific mouse vascular beds. (A) Representative images of confocal immunofluorescence of PECAM-1 (green) and EMMPRIN (red) in sections of mouse spleen, kidney (G: glomerulus), lung, heart and brain. Arrows point to colocalization of EMMPRIN with PECAM-1 at endothelial junctions. Scale bars: 10μm. (B) Representative whole-mount confocal immunofluorescence of PECAM-1 (green) and EMMPRIN (red) in mouse ear and aorta. Arrows point to colocalization of EMMPRIN with PECAM-1 at endothelial junctions. Scale bars: 20 μm.

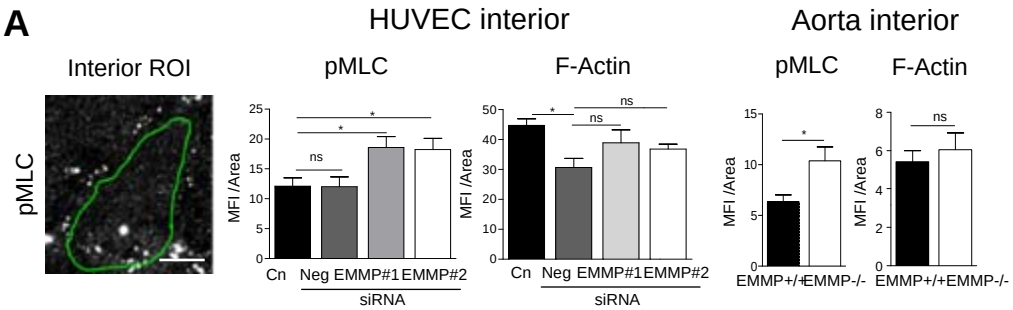
A
HUVEC interior
Aorta interior
Interior ROI
pMLC
F-Actin
pMLC
F-Actin
MFI /Area
Cn
Neg
EMMP#1
EMMP#2
siRNA
EMMP+/+
EMMP-/-
ns

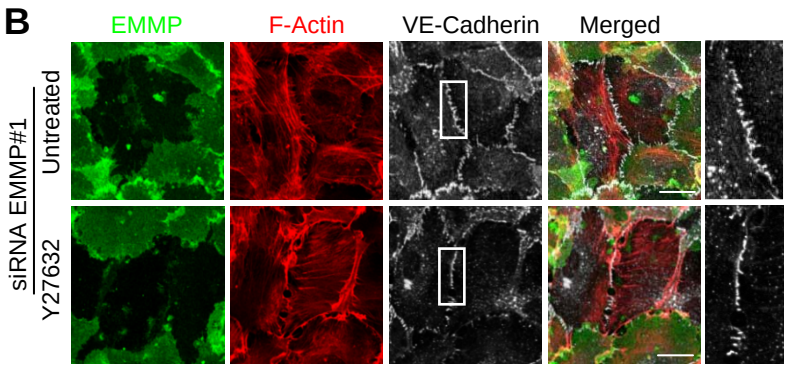
B
EMMP
F-Actin
VE-Cadherin
Merged
siRNA EMMP#1
Untreated
Y27632

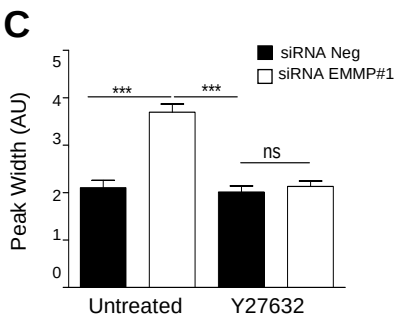
C
siRNA Neg
siRNA EMMP#1
Peak Width (AU)
Untreated
Y27632
ns

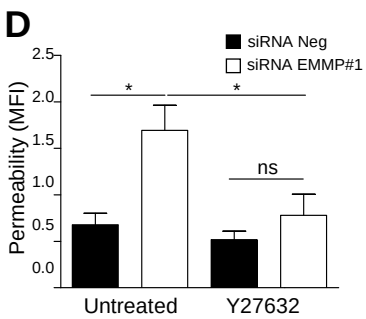
D
siRNA Neg
siRNA EMMP#1
Permeability (MFI)
Untreated
Y27632
ns

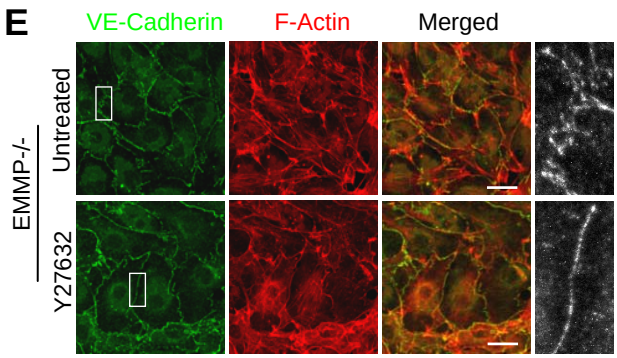
E
VE-Cadherin
F-Actin
Merged
EMMP-/-
Untreated
Y27632

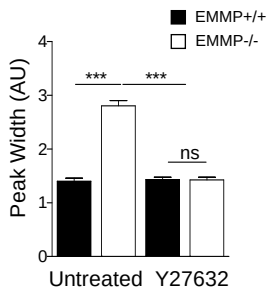
F
EMMP+/+
EMMP-/-
Peak Width (AU)
Untreated
Y27632
ns

Fig. S2. Relaxation of the actomyosin machinery rescues the VE-cadherin pattern in EMMPRIN-deficient MLEC. (A) Interior regions of interest (ROI) were drawn as the area delineated in the representative image for pMLC staining (left). Scale bar: 20μm. Histograms show quantification of mean fluorescence intensity (MFI) for pMLC and F-actin at the interior of control and EMMPRIN-interfered HUVEC or wildtype and EMMPRIN-deficient aortas (right); n=30-40 junctions were quantified in 2-3 independent experiments per condition (*P<0.05, **P<0.01, ***P<0.001). (B) Representative images of EMMPRIN-interfered HUVEC treated as indicated with the Rho kinase inhibitor Y27632. Cells were stained for EMMPRIN (green), F-actin (phalloidin; red) and VE-cadherin (white). Magnified views of the boxed areas show detail of the VE-cadherin pattern. Scale bars: 20μm. (C) Quantification of VE-cadherin width at the junctions formed by control and EMMPRIN siRNA-interfered HUVEC treated or not with Y27632. Around 40 junctions were quantified in each group (***P<0.0001). (D) Quantification of monolayer permeability in negative siRNA and EMMPRIN siRNA-interfered HUVEC treated with Y27632 (**P<0.01). (E) MLEC from wildtype or EMMPRIN-null mice were untreated or treated with Y27632 and stained for VE-cadherin (green) and F-actin (phalloidin; red). Magnified views of the boxed areas show detail of the VE-cadherin pattern. Scale bars: 20 μm. (F) The histogram shows quantification of VE-cadherin width at the junctions in each condition (***P<0.0001). 20-30 junctions were analyzed in MLEC from two animals per genotype.

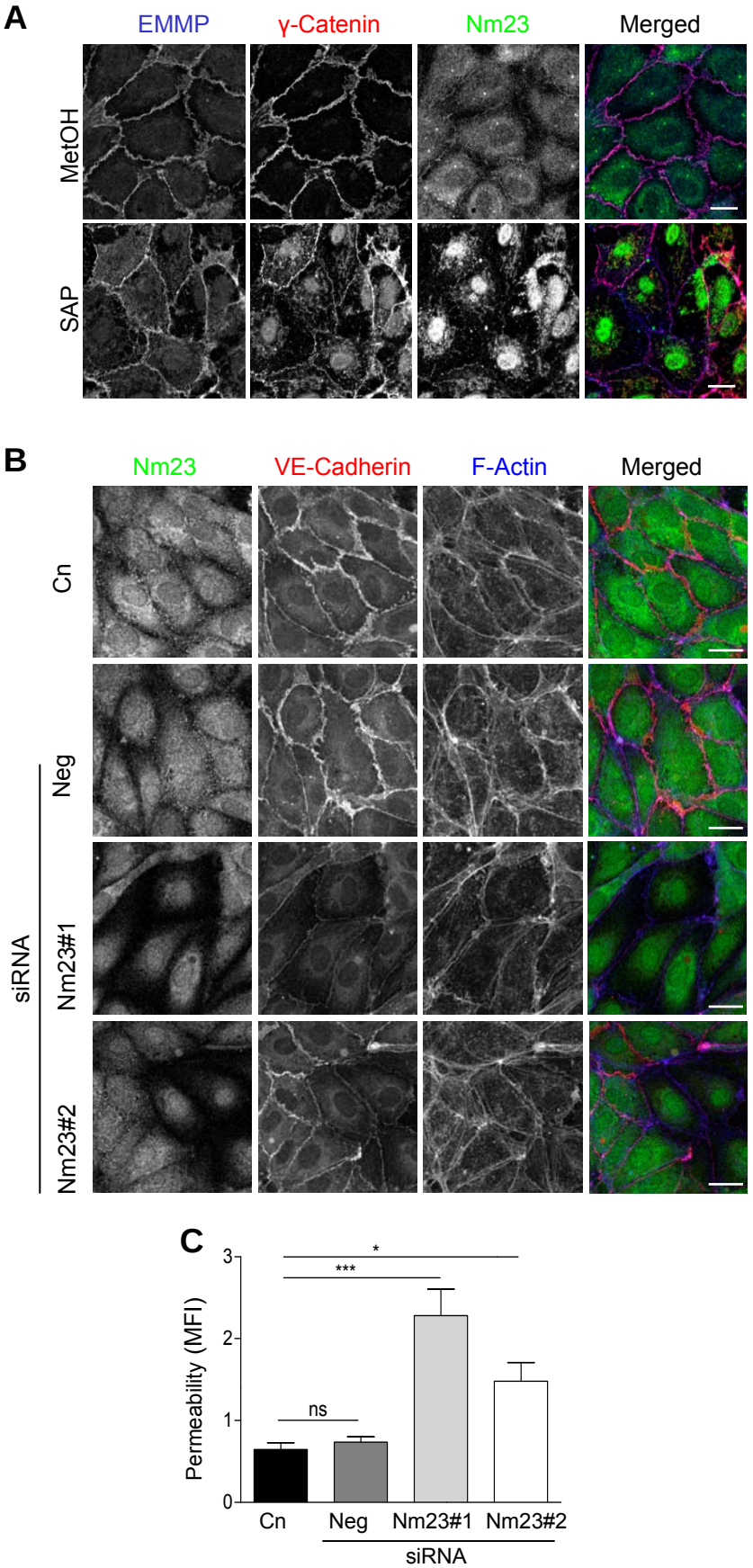

Fig. S3. Nm23 is associated with EMMPRIN/γ-catenin at endothelial junctions and required for their integrity. (A) Representative confocal sections in B&W of EMMPRIN (blue), γ-catenin (red) and Nm23 (green) staining in HUVEC under different fixation conditions. SAP: saponin. Images are confocal sections of 0.3µm. Scale bars: 20 µm. (B) Representative images are shown in B&W of staining for Nm23 (green), VE-cadherin (red) and F-actin (phalloidin; blue) in Nm23 siRNA-interfered HUVEC. Scale bars: 20 µm. (C) Graph shows permeability values for monolayers of HUVEC interfered as indicated. Data are the means ± SEM of the amount of labeled dextran recovered in the lower chamber after 1 h (n=4 independent

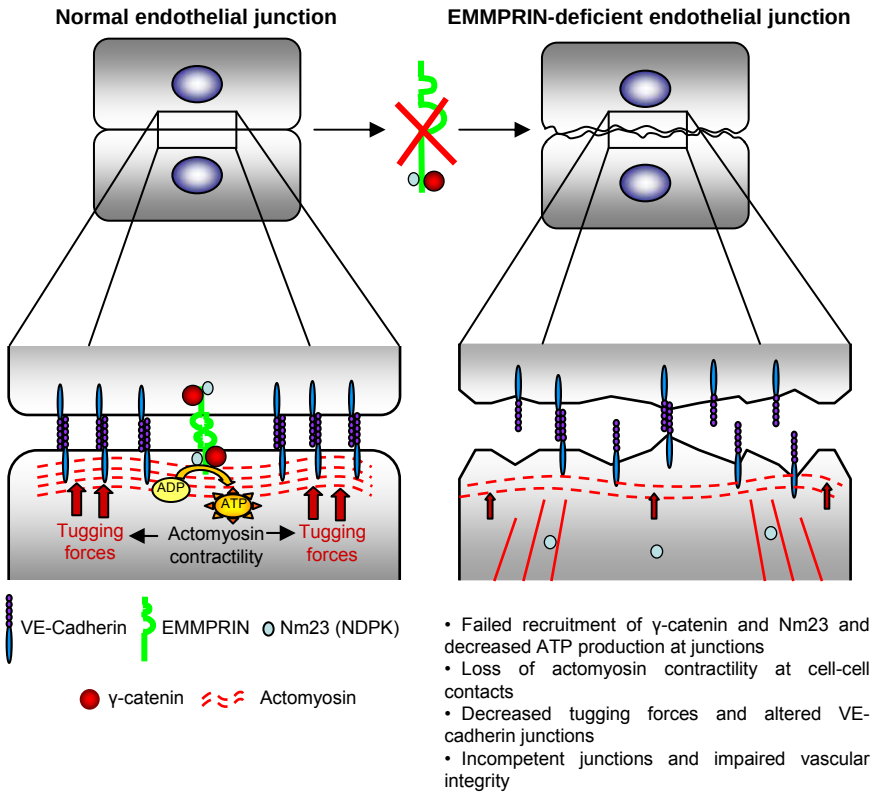

Fig. S4. EMMPRIN/γ-catenin/Nm23 complex is required for endothelial junction integrity. At endothelial cell junctions, EMMPRIN associates with and recruits γ-catenin and the nucleoside diphosphate kinase Nm23, which, by producing ATP, regulates MLC phosphorylation, actomyosin contractility and tugging forces at these sites. In the absence of EMMPRIN, failed γ-catenin and Nm23 recruitment at junctions results in decreased ATP and actomyosin contractility, reduced tugging forces and impaired endothelial junctional competence in vitro and in vivo.

Supplementary Movies

Movies 1 and 2. EMMPRIN is required for F-actin bundle formation during endothelial junction maturation. EMMPRIN–expressing and EMMPRIN-knockdown HUVEC were transfected with LifeAct (red) for F-actin visualization, stained with EMMPRIN-Alexa 488 (green) and time-lapse recorded for 18 h.

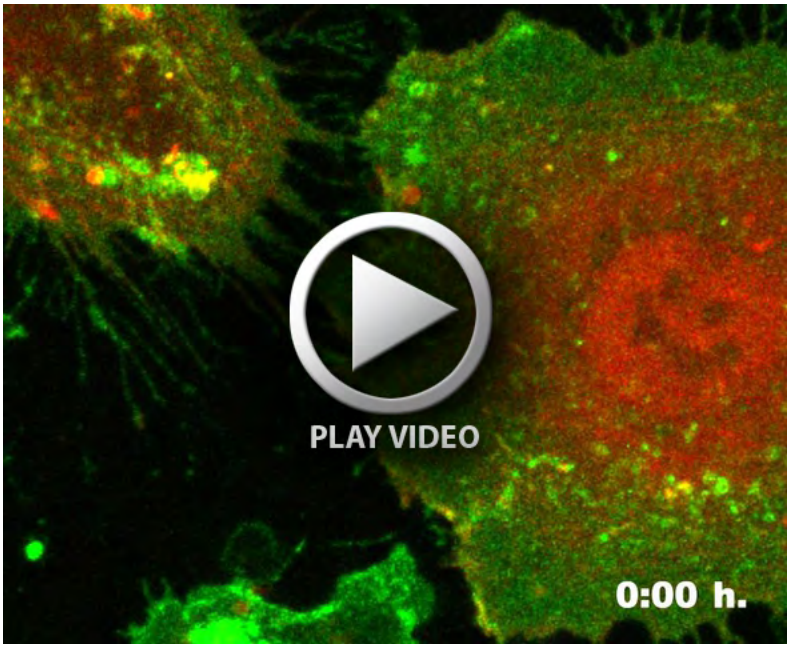

Movie 1.

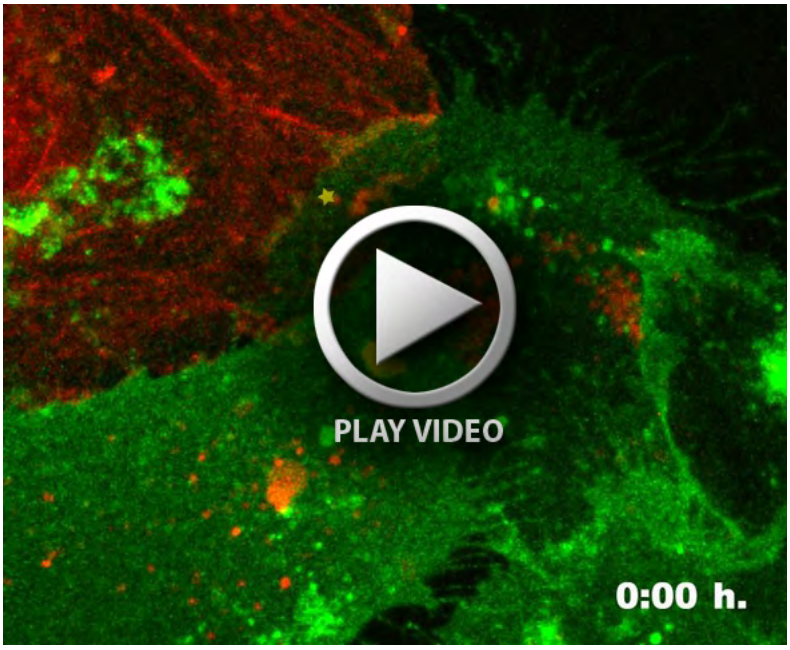

Movie 2.